Editorial Manager(tm) for PLoS Biology
Manuscript Draft

Manuscript Number:

Title: High-Resolution Quantification of Focal Adhesion Spatiotemporal Dynamics in Living Cells

Short Title: Quantifying Focal Adhesion Dynamics

Article Type: Research Article

Keywords: focal adhesions; computer vision; high-content analysis

Corresponding Author: Shawn M. Gomez

Corresponding Author's Institution: University of North Carolina at Chapel Hill

First Author: Matthew E. Berginski

Order of Authors: Matthew E. Berginski;Eric A. Vitriol;Klaus M. Hahn;Shawn M. Gomez

Abstract: Focal adhesions (FAs) are macromolecular complexes that provide a linkage between the cell and its external environment. In a motile cell, focal adhesions change size and position to govern cell migration, through the dynamic processes of assembly and disassembly. To better understand the dynamic regulation of focal adhesions, we have developed an analysis system for the automated detection, tracking, and data extraction of these structures in living cells. This analysis system was used to quantify the dynamics of fluorescently tagged Paxillin and FAK in NIH 3T3 fibroblasts followed via Total Internal Reflection Fluorescence Microscopy (TIRF). High content time series included the size, shape, intensity, and position of every adhesion present in a living cell. These properties were followed over time, revealing adhesion lifetime and turnover rates, and segregation of properties into distinct zones. We show how a single point mutation in Paxillin at the Jun-kinase phosphorylation site Serine 178 changes FA size, distribution, and rate of assembly. This study provides a detailed, quantitative picture of FA spatiotemporal dynamics as well as a set of tools and methodologies for advancing our understanding of how focal adhesions are dynamically regulated in living cells.

Suggested Reviewers:

Opposed Reviewers:

Cover Letter

Joint Department of Biomedical Engineering
The University of North Carolina at Chapel Hill and
North Carolina State University at Raleigh

152 MacNider Hall, Chapel Hill, NC 27599-7575
(919) 966-1175; (919) 966-2963 fax
http://www.bme.unc.edu

2147 Burlington Laboratories, Raleigh, NC 27695-7115
(919) 515-5252; (919) 513-3814 fax
http://www.bme.ncsu.edu

December 2, 2010

PLoS Biology
Public Library of Science
185 Berry Street, Suite 3100
San Francisco, CA 94107

Dear PLoS Biology editors:

Please consider this revised manuscript titled "High-Resolution Quantification of Focal Adhesion Spatiotemporal Dynamics in Living Cells" by Matthew E. Berginski, Eric A. Vitriol, Klaus M. Hahn and Shawn M. Gomez for publication in *PLoS Biology.* We note that this is a previous interaction (10-PLBI-RA-6319). We greatly appreciate the reviewer's thoughtful comments and have tried to thoroughly address their questions and concerns.

Highlights of some of our changes relative to specific reviewer comments follow below. A full, point-by-point response is included after this summary section:

- Reviewer 1 had a major concern regarding the availability of the software, stating that "*Taken together, I would recommend acceptance of the paper, under the condition that the software is made available to the scientific community (ideally – downloadable from the Journal's website).*"
    - We were not clear enough in our original submission and have clarified it in this revision – the software is freely available under an open-source license and can be downloaded from our lab website (http://gomezlab.bme.unc.edu/tools) and includes documentation and sample data on which the software can be run. In addition, we would be happy to have the software available on the PLoS' website. Continued updates to the software will be made available on the lab website.
    - A number of other concerns were also addressed.
- Reviewer 2 was perhaps most interested in us elucidating the mechanisms and role of the phosphorylation event on Paxillin that we describe. While we do agree that this is a very interesting and important area worth pursuing, it was not the main focus of this manuscript. We have addressed all other Reviewer concerns as well as possible and have further altered the title to deemphasize the "key regulator" aspect of the S178 Paxillin mutant used in this work.
- Reviewer 3 was very favorable towards the work, with the primary critique being to provide supporting measurements using another adhesion marker. We used FAK as an alternative marker of adhesions, replicating relevant aspects of the statics and dynamics analysis using this marker. We found identical rates of assembly and disassembly for adhesion regardless of whether Paxillin or FAK was used as the adhesion marker.

Again, we greatly appreciate the reviewers' comments and questions and feel that they have greatly improved the quality of the manuscript. We would like to use the same list of potential reviewers identified in our prior interaction (10-PLBI-RA-6319). We believe this work provides a novel picture of adhesion dynamics in living cells as well as a tool for use by the broader adhesion research community. We look forward to moving ahead towards publication of this manuscript.

Sincerely,

Shawn M. Gomez & Klaus M. Hahn
School of Medicine, UNC-Chapel Hill

Manuscript
Click here to download Manuscript: FA_paper.pdf

High-Resolution Quantification of Focal Adhesion Spatiotemporal Dynamics in Living Cells

Mathew E. Berginski[1,*], Eric A. Vitriol [2,*], Klaus M. Hahn[4,5], & Shawn M. Gomez[1,3,4]

[1]Department of Biomedical Engineering, [2]Department of Cell and Developmental Biology, [3]Department of Computer Science, [4]Department of Pharmacology, and [5]Lineberger Comprehensive Cancer Center, University of North Carolina, Chapel Hill, North Carolina 27599, USA

Correspondence to: Klaus M. Hahn[4,5] (khahn@med.unc.edu) and Shawn M. Gomez[1,3,4] (smgomez@unc.edu)

[*]these authors contributed equally to this work

Short Running Title:

Quantifying Focal Adhesion Dynamics

Keywords:

focal adhesions; computer vision; high-content analysis

Abstract

Focal adhesions (FAs) are macromolecular complexes that provide a linkage between the cell and its external environment. In a motile cell, focal adhesions change size and position to govern cell migration, through the dynamic processes of assembly and disassembly. To better understand the dynamic regulation of focal adhesions, we have developed an analysis system for the automated detection, tracking, and data extraction of these structures in living cells. This analysis system was used to quantify the dynamics of fluorescently tagged Paxillin and FAK in NIH 3T3 fibroblasts followed via Total Internal Reflection Fluorescence Microscopy (TIRF). High content time series included the size, shape, intensity, and position of every adhesion present in a living cell. These properties were followed over time, revealing adhesion lifetime and turnover rates, and segregation of properties into distinct zones. We show how a single point mutation in Paxillin at the Jun-kinase phosphorylation site Serine 178 changes FA size, distribution, and rate of assembly. This study provides a detailed, quantitative picture of FA spatiotemporal dynamics as well as a set of tools and methodologies for advancing our understanding of how focal adhesions are dynamically regulated in living cells.

Author Summary

Focal adhesions are dynamic protein complexes that mediate the connection between cells and their external environment, and are intimately connected to processes such as cellular motility. Images of cells with fluorescently labeled adhesion proteins are often used to assess the effects of system perturbations on adhesion development and function. Traditional methods that use these images to characterize and quantify the effects of various perturbations on focal adhesions typically involve manual identification, tracking and assessment of focal adhesion properties. As a result, the number of adhesions that can be studied, as well as the breadth and resolution of properties quantified, has been significantly limited. In this work, we describe a computational analysis system that automates the collection and quantification of focal adhesion properties with an order of magnitude or more increase in the number of adhesions characterized, and with corresponding improvements in the quantification of their properties. This system was used to quantify the dynamics of two key adhesion components, Paxillin and Focal Adhesion Kinase (FAK). We also compared the dynamics of Paxillin in its wild-type state against a single amino acid mutation known to disrupt Paxillin's regulation by Jun N-terminal Kinase. Results of this analysis demonstrate that this interaction between Paxillin and Jun N-terminal Kinase has major effects on focal adhesion dynamics, helping to explain earlier results describing impaired cell movement as well as demonstrating the benefits of the new analysis approach in quantifying adhesion dynamics within living cells.

Introduction

Focal adhesions (FAs) are dynamic, multi-component protein complexes that serve as points of integration for both mechanical and chemical signaling, while playing a central role in a

variety of processes including cancer metastasis, atherosclerosis and wound healing [1,2,3]. Characterizing how these structures dynamically change is essential for understanding cell migration, which requires that adhesions are continuously remodeled as the cell moves forward. During motility, new adhesions are born at the leading edge of a protruding lamellipodia. They then enlarge and are either disassembled at the base of the protrusion in a process known as adhesion turnover, or become longer-lived structures that are eventually dismantled in the retracting tail at the rear of the cell [4,5,6]. In this cycle as well as other FA-mediated processes, FA dynamics are highly regulated by structural and signaling molecules [7,8,9]. Alterations in the balance of these regulating factors plays a key role in adhesion turnover and thus in adhesion signaling and normal cell function.

Microscope imaging of FAs has driven a significant portion of our current understanding of adhesion dynamics, with methods such as total internal reflection fluorescence microscopy (TIRF) providing high-resolution images suitable for quantitative analysis. However, challenges in image capture and downstream analysis have generally led to the characterization of only a relatively small number of hand-picked adhesions within any given cell [7,8,10,11,12]. Recent technical and methodological improvements have allowed for the automated detection and characterization of focal adhesions for high-throughput screening studies. For instance, Paran and colleagues [13] have reported on the use of a high-throughput high-resolution imaging system to screen a plant extract library for effects on adhesion morphology and distribution. The same high-throughput imaging system was used to perform multicolor analysis on various adhesion components [14] and this system was used in an siRNA screen against adhesion related genes [15]. In these studies, researchers were able to obtain molecular signatures of protein components within focal adhesions, resolve sub-domains within adhesions, and identify clusters

of genes that had similar effects on focal adhesion morphology and placement. These studies demonstrate the power of identifying and characterizing all adhesions within a cell. However, as the approaches used in these studies relied on cell fixation, critical aspects of focal adhesion biology, including their spatiotemporal dynamics, were lost.

Here, we describe a novel system for the quantification of focal adhesion dynamics. This approach utilizes high-resolution (60x oil-immersion) time-series images of living cells generated with TIRF. Image sequences are processed through an analysis system that identifies each individual adhesion, tracks their movement through time and collects associated properties concerning the location, shape, size and intensity. As the birth, lifetime and death of each adhesion is quantified in this approach, a thorough picture of global adhesion spatiotemporal behavior is captured.

To demonstrate the power of this approach, we focus on the molecular scaffold protein Paxillin, a core constituent of focal adhesions. Through direct interactions with both structural and regulatory components, Paxillin serves as a platform for adhesion signal transduction [16]. A principal regulatory mechanism of Paxillin is phosphorylation, with over 40 sites of phosphorylation currently identified [9]. The roles of many of these phosphorylation sites have yet to be characterized, but many of those that have been studied demonstrate strong effects on cell migration. Of particular interest is the c-Jun N-terminal kinase (JNK) phosphorylation site Serine 178 (S178). Preventing JNK phosphorylation through mutation of this Serine to Alanine, or by inhibition of JNK signaling, inhibits cell motility [17,18]. More recently, it has been shown that phosphorylation of S178 enhances Paxillin's interaction with FAK, resulting in tyrosine phosphorylation at residues 31 and 118 [19]. Furthermore, expression of the phosphomimetic Y31D/Y118D Paxillin can rescue the S178A mutant phenotype. This and related work suggests

that JNK phosphorylation of Paxillin may be an important early step in adhesion formation.

In this study, we use our imaging analysis system to characterize FAs labeled with EGFP-Paxillin, generating high-resolution data sets of adhesion distribution, morphology, and turnover in migrating NIH 3T3 fibroblasts. The results demonstrate that we can analyze adhesions in an unbiased manner, with 10^3-10^4 adhesions analyzed per cell. With wild-type Paxillin as a baseline for comparison, we use our system to detect alterations in adhesion spatiotemporal properties in response to S178 mutation. Through this analysis we show that the loss of this single phosphorylation site affects adhesion site formation, size and assembly rates. We also verify the broad applicability of the analysis system by also applying the methods to examine time-lapse movies of EGFP-FAK. We are also making the analysis system available under an open source license, to allow the community use our methods to analyze new experimental systems. Additionally, these results illustrate the benefit of capturing large quantitative data sets that allow subtle differences to be easily detected. These results further improve our understanding of JNK regulation of Paxillin and focal adhesion dynamics, as well as demonstrating the utility of appropriately designed image analysis systems in the characterization and analysis of high-content data sets.

Results

Quantitative Analysis of Focal Adhesion TIRF Images

To quantify aspects of focal adhesion spatiotemporal dynamic behavior, we generated an NIH 3T3 fibroblast cell line expressing both EGFP-Paxillin, to label FAs, and a myristoylated-Red Fluorescent Protein (myr-RFP), to identify the cell edge. Cells were plated on fibronectin and imaged with TIRF for 1-4 hours. We quantified FA dynamics through a multistage image

analysis pipeline (Figure 1). Briefly, FAs were identified and segmented with a watershed-based algorithm (see Methods). Static properties of adhesions identified and quantified at each timepoint included properties such as area, position and fluorescent Paxillin intensity. Dynamic properties of adhesions, such as velocities and changes in fluorescent intensity, were determined by tracking and measuring adhesion properties across time steps/images. At each consecutive time step, adhesion birth and death events were identified and recorded by the software.

An example of the segmentation results and static properties are shown in Figure 2. The segmentation methods successfully identify the adhesions in each image regardless of the background Paxillin fluorescence intensity (Figure 2A, B). The dynamic nature of the adhesions during this sample experiment is clear when all the adhesions identified are shown superimposed in a single image (Figure 2C). The static properties show several general properties of the adhesions in wild-type cells (Figure 2D). In general, adhesions are less than $0.2\mu m^2$ in size, have axial ratios less than 3 and exist for less than ten minutes, although there are many adhesions that live longer. Both Paxillin fluorescence intensity and the position of the adhesion centroids with respect to the cell edge have skewed distributions. Quantifying properties for over 44,000 adhesions, these results demonstrate the capabilities of our system to provide high-resolution and unbiased assessment of FA behavior.

Kinetics of FA Assembly and Disassembly

Of particular importance for understanding FA functions is the assessment of adhesion behavior through time. Figure 3A-D shows the methods used in determining FA assembly and disassembly rates for individual adhesions. Figure 3A depicts an image series of a single adhesion (highlighted in green) from birth, through maturation and stability, and on to death.

Using time series information, we quantified the normalized intensity of each adhesion over its lifespan (Figure 3B). Readily apparent are the log linear assembly and disassembly phases, which are automatically fit to a log linear model (see Methods for details). Our results are consistent with previous work showing that adhesions assemble and disassemble with log linear progression [7]. Specifically, we observed that the assembly and disassembly curves of over 50% of all adhesions analyzed (n = 1183 for assembly and n = 1487 for disassembly) could be described by a log-linear fit, showing R^2 values of 0.79 or better (Figure S1). Note that the smaller number of adhesions analyzed relative to the statics properties of Figure 2 is due to the need for a minimum adhesion lifetime as well as other requirements for accurate quantification of rates (see Methods). In the example shown in Figure 3, a log linear approximation describes 90.5% and 96.1% of the variance in the rates of intensity increase and decrease, respectively (Figure 3C, D). In between these two phases we define a stationary/mature phase where intensity remains relatively stable (Figure 3B).

We used our system to characterize the rates of FA assembly and disassembly by repeating the analysis detailed in Figure 3A-D on all adhesions identified by our software (n = 21 cells). Results were focused on FAs having lifetimes of at least 20 minutes, where the detected assembly or disassembly rate is positive and the p-value of the rate model is below 0.05 (see methods for details, Figure 3E). The mean rate of assembly of 0.031±0.023 min^{-1} is 55% greater than that of disassembly (0.020±0.014 min^{-1}). While these average rates are slower than earlier published reports, the values determined in previous studies were estimated from far fewer measurements and can be found within the variance of our data set. Thus, this automated computational approach provides a comprehensive picture of the breadth of adhesion assembly and disassembly dynamics without biasing analysis toward any particular subset.

Spatial Properties of FA Assembly and Disassembly

In addition to estimation of assembly and disassembly rates, the analysis pipeline also collects spatial properties of FAs, allowing spatial aspects of FA behavior and dynamics to be similarly studied. Using the same set of experiments used to determine the kinetics of assembly and disassembly, we asked where adhesions originate and die (Figure 4). The majority (63%) of adhesions are born less than 5μm from the cell edge, with a mean distance from the edge at birth of 6.34μm (Figure 4A). In contrast, adhesions tend to die further from the edge with only 27% of adhesions dying within 5μm of the edge (Figure 4B). The mean distance from the edge at adhesion death was 9.5μm. This suggests the existence of two distinct, but partially overlapping "zones" within which preferential birth or death of FAs occurs. When looking at both FA birth/death location and assembly/disassembly rate simultaneously, we find that higher assembly rates are observed in births that occur near the edge while no obvious effect of spatial location on the rate of disassembly is apparent (Figure 4).

Analysis of EGFP-labeled FAK adhesions

To verify that the statics and dynamics analysis methods could be applied to study other FA protein properties, we expressed FAK labeled with EGFP. After gathering 10 time-lapse movies tracking the position of FAK in MEFs using TIRFM, we applied the same set of algorithms to determine the assembly and disassembly rate of the FAs. The rates of assembly and disassembly of FAs were found to be identical when comparing labeled Paxillin to labeled FAK in live cells (Figure 5). This result indicates that the rate (or “flow”) of Paxillin and FAK into and out of a focal adhesion is identical. In contrast, subtle but statistically significant differences

in adhesion areas and axial size were found when comparing EGFP-Paxillin vs EGFP-FAK labeled adhesions (

Figure **S2**). This result is not unexpected as different spatial and/or stoichiometric relationships are expected for both Paxillin and FAK within FAs. These results further support the capability of this system to be generally applicable to the measurement of other adhesion components besides Paxillin.

Paxillin S178A Mutant Perturbation

The previous results establish the ability of our approach to quantify static, dynamic and spatial properties of adhesions. Furthermore, the ability to identify and characterize very large numbers of adhesions provides the potential to detect changes in adhesion phenotype that are difficult or impossible to characterize manually. Using the FA analysis pipeline, we investigated the effect of a Paxillin mutation (Serine 178 to Alanine) on several aspects of FA behavior. As discussed earlier, this mutation blocks JNK phosphorylation of Paxillin and has known effects on cell motility. However, the effects of this mutation on adhesion dynamics have not been well characterized.

We found that the S178A mutation induced a number of significant effects on the morphological, dynamic and spatial properties of adhesions. The mean area of the S178A mutant adhesions are decreased by 23%, while the mean axial ratio decreases by 5% in the S178A mutants (Figure 6). Perhaps most relevant to the observed alterations in cell motility, there is an approximately 42% reduction in the median rate of adhesion assembly (Figure 7A). We also observe a smaller (30%) but statistically significant decrease in median *disassembly* rate (Figure 7B). Thus, the kinetics of FA assembly and disassembly are strongly affected by this mutation,

but in a non-symmetric manner.

We previously observed that adhesions in wild-type cells have different distributions of birth and death positions relative to the cell edge. In comparison to WT cells, we find that the median distance from the edge at birth is greater by 30% in S178A mutants (Figure 7C). There is no significant difference between WT and mutant cells with regard to where an adhesion dies, suggesting that spatial aspects of the disassembly process (i.e. where disassembly occurs) is not dependent and/or sensitive to JNK phosphorylation (Figure 7D).

Finally, we compared the length of time spent in the assembly, stationary, and disassembly phases for cells expressing either WT or S178A EGFP-Paxillin. Results suggest that the S178A mutation causes adhesions to be longer-lived, spending a greater amount of time in the assembly phase than WT cells and lesser time in the disassembly phase (Figure 8). There is no difference in time spent in the stability phase. As a whole, our results demonstrate the most pronounced effects of the S178A mutation occur in the assembly phase: position at birth, assembly rate, and time spent assembling.

Discussion

We have described the development of a set of computational tools suitable for the global characterization of FA spatiotemporal dynamics and assessing the results of network perturbation on adhesion properties and behavior. The S178A mutation was presented as a case study in applying these tools for analyzing complex FA phenotypes. Through this analysis, we were able to show that adhesion dynamics fall into distinct behavioral subtypes occurring in different regions of the cell, and that the S178A Paxillin mutant causes significant changes in FA

assembly and disassembly, providing a mechanism for previously observed migration defects. These changes indicate that Jun Kinase, via Paxillin, strongly controls the FA lifecycle.

The computational tools presented allow the entire FA life span to be analyzed. These tools include an automated adhesion detection, segmentation and tracking system; extracting a range of properties valuable for understanding FA development. All of these methods were tested using simulated data that replicated many of the observed experimental processes, confirming these methods are able to accurately quantify adhesion properties under controlled conditions (see Figure S11-Figure S13 and methods). The differences detected between the wild-type and S178A mutants are robust, being preserved through a range of parameter choices for the adhesion detection limit and the minimum length of the assembly and disassembly phases. The rate at which images were taken in this work (1 sample/min) also appears to be over the sampling rate needed to accurately measure the assembly and disassembly rates of long-lived adhesions (Figure S9-Figure S10).

Our analysis system integrates methods for automatically identifying and extracting rates of FA assembly and disassembly. We find that the assembly and disassembly rates detected using these automated methods encompass the rates determined using manual methods [7], while quantifying vastly greater numbers of adhesions. We also find that adhesions labeled with an alternate adhesion marker, FAK, also allows a similar number of adhesions to be quantified and that these adhesions are similar to those detected using fluorescently labeled Paxillin. Differences in the mean rates detected by manual versus automated searches can be attributed to several factors. First, the rates determined using manual methods originate from user-specified adhesions of interest. Such adhesions may be chosen based on specific localization properties, such as selecting only those adhesions found within particular cell regions, while the presented

results do not make any distinction between adhesions present in different cellular structures *a priori* (though the properties of adhesions at particular locations can be determined *a posteriori*). In addition, due to our emphasis on observing the birth, death and taking multiple samples during the assembly and disassembly phase of an individual adhesion, our rate analysis focused on long-lived adhesions, which might have different properties than those measured in studies of short-lived adhesions. Finally, as our software analyzes all adhesions regardless of the brightness of the adhesion, we avoid biases that may occur through, for example, preferential selection of large or highly visible adhesions. Thus, the automated methods described here greatly extend the types of adhesions that can be analyzed, as well as the range of properties that can be quantified.

The spatial properties of FA birth and death suggest that FAs have distinct regions where assembly and disassembly events are most concentrated. These assembly and disassembly regions overlap, but remain distinct. The greatest concentration of assembly events occur within 5μm of the cell edge. Previous studies in the same cell line indicate that this 5μm range coincides with the end of the lamellipodia and the beginning of the lamella, where the structure of the actin cytoskeletal network changes significantly. Recently published data indicate that this transition, where stable actin structures differentiate into branched structures that exert force on the leading edge for protrusion, is determined by interactions between the cytoskeleton and adhesion proteins[20]. Further investigation will be required to more fully interpret this observation.

Our analysis enabled us to quantify differences in FA dynamics caused by mutation of Paxillin at a JNK phosphorylation site. Both adhesion assembly and disassembly were affected. In addition to these strong perturbations, more subtle changes in FA dynamics and localization were also detected, including a decrease in adhesion size. In agreement with our results, a recent

siRNA screen of FA proteins within fixed cells that included JNK knockdown also measured decreases in adhesion size [15].

Based on our results, a summary model of the FA lifecycle in both wild-type and S178A cells is depicted in Figure 9. Shown to scale, the S178A mutation shows distinct effects on both the assembly and disassembly phases of FA development, but these effects are different in magnitude. Determining what FA development signals are involved in perturbing assembly, stability and disassembly is an ongoing process, but these proof of principle TIRF experiments demonstrate the capabilities of the software analysis system to make biologically significant new observations.

Development of new and/or improved analysis modules is ongoing. In prior studies, analysis of the cell edge velocity has proven to be a robust phenotype that can be used to quantify the effect of many different perturbations to the signaling networks that control cellular motility [21]. Integration of this type of data will allow the rates of cell edge movement to be analyzed in terms of FA phenotypes. Such studies will help to bridge the gap between FA dynamics and the well-developed fields of cell edge and cytoskeletal dynamics. The data sets collected using the software also provide information about the specific properties of the adhesions during each phase of their lifecycle. While the "distance from cell edge" measure used here displays interesting relationships, the application of more powerful spatial statistics methods will allow the more rigorous quantification of spatial, as well as spatiotemporal properties. Such spatial methods will also be important to understanding polarized cell behaviors.

In summary, we have described a system for quantifying the spatiotemporal dynamics of FAs, generating highly-detailed descriptions of FA behavior based on large populations, and further enabling high-content screening methods to be applied to understanding the perturbation

of FA signaling networks. The system was applied to quantifying the differences in FA development generated through a single amino acid mutation of the FA scaffolding protein Paxillin. Future studies of other FA perturbation methods with high-content analysis methods should provide a comprehensive picture of the role of FA signaling proteins in the control of FA development and localization.

Methods

Cell Culture

NIH 3T3 fibroblasts (MEFs) and 293 LinXE ecotropic packaging cells were cultured in 5% CO_2 at 37℃ in Dulbecco's modified Eagle's medium (DMEM, Mediatech) supplemented with 10% fetal calf serum, 1% L-Glutamine, and 1% penicillin-streptomycin. Fibroblasts were imaged in Ham's F-12K medium without phenol red (SAFC Biosciences) with 2% fetal bovine serum, 15mM HEPES, 1% L-Glutamine, and 1% penicillinstreptomycin.

To make stable cell lines, retroviral vectors were transfected into 293 LinXE cells plated in 6cm dishes with Fugene 6 (Roche) according to the manufacturer's protocol (using 18μL of Fugene 6 and 4.5μg of DNA). The media was replaced after 12 hours. Viral supernatant was harvested 48 hours after media replacement, passed through a .45μm syringe filter and then added to MEFs plated at subconfluent densities at a ratio of 1:3 (viral supernatant/normal media). Cells were infected for several rounds until they reached expression levels sufficient for live cell imaging. No differences were detectable in the expression levels of the EGFP-Paxillin and EGFP-PaxillinS178A constructs (Figure S3).

Microscopy

Prior to imaging, MEFs were plated onto coverslips coated with 5μg/mL Fibronectin (Sigma) for 30min. Fibroblasts expressing EGFP-PaxS187A required 2-3 hours to adhere to the coverslips due to a spreading defect. Immediately before being transferred to a sealed imaging chamber, complete culture media was replaced with imaging media. Imaging experiments for all cells used in this study were conducted within the first 8 hours after plating.

Imaging was performed on an Olympus IX81 motorized inverted microscope equipped with a ZDC focus drift compensator and a TIRFM illuminator, a 60X 1.45 NA PlanApoN TIRFM objective, a cooled digital 12-bit CCD camera (CoolSnap, Roper Scientific), a 100W Mercury arc lamp, and MetaMorph imaging software. The 488nm laser line from a Krypton-Argon ion laser (Series 43, Omnichrome) was controlled with a custom laser launch/AOTF (LSM Technologies). Imaging of the cells expressing EGFP-FAK was performed on a Nikon Eclipse Ti inverted microscope equipped with the Perfect Focus System, a TIRF illuminator, a 60X 1.45NA PlanApoN TIRF objective, a a cooled digital 16-bit EMCCD camera (QuantEM: 512SC, Photometrics), an Argon ion laser (Melles Griot) controlled with a custom laser launch/AOTF, and Nikon Elements imaging software. Images were acquired with 2 x 2 binning, except for images of EGFP-FAK expressing cells, which were acquired with 1 x 1 binning. Illumination intensity was controlled with either the AOTF (TIRF excitation) or neutral density filters (epifluorescence excitation.Simultaneous TIRF images of EGFP and epifluorescence images of RFP were acquired using an 80/20 (TIRF / Epifluorescence) splitter mirror, a custom dichroic mirror (Chroma) and the following band-pass filters: EGFP (HQ 525/50); RFP (HQ580/30, HQ 630/40).

Image Processing

Methods to identify individual FAs were adapted from [22], with some modification. Briefly, each image taken during an experiment was high pass filtered, using a round averaging filter with a radius of 11 pixels (4.95μm diameter). The high pass filtered images were threshholded by an empirically determined value set to identify adhesion pixels. The water segmentation method was used as described, but with the following modifications. When a pixel acts as bridge between two large adhesions, where large is defined as 40 or more pixels (1.85μm^2), the bridge pixel is assigned to the adhesion whose centroid is closest to the bridge pixel. Also, holes in any single adhesion were filled using the same water segmentation algorithm. Between 200 and 600 adhesions were found in each image from the experimental data. After each focal adhesion has been identified, static adhesion properties are then collected.

Cell edges were found by analyzing the myr-RFP images using a method similar to that described in a prior publication [23]. This method automatically identifies a single threshold which splits the myr-RFP images into cell body and background regions. Briefly, a histogram of all the intensity values for a single image was collected and split into 1000 equal sized bins. The counts of each bin were then smoothed with the loess algorithm (Polynomial order 2, 5% of data included in each fit). This smoothed histogram has two peaks corresponding to the background region and the cell body. The local minima and maxima in the smoothed histogram are found and the two maxima at the lowest pixel intensity bins identified. The threshold for image segmentation is set to the minima between the set of maxima found in the prior step. After thresholding the image, the connected regions are identified and the regions less than 10 pixels in area are discarded. The cell edge is defined by the border pixels of the connected regions.

FA Tracking

With the focal adhesions identified in each image of the experimental data set, another series of algorithms were designed to track the focal adhesions through each sequential image. The tracking algorithm is based on a birth-death model of a FA lifetime (Figure S4). In each sequential image a FA can either be born, continue into the next time step, merge or die. The birth-death-merge processes are detected by examining the properties extracted from the segmented adhesions. The results of this tracking algorithm are assignments of the FAs identified in each image into lineages that track the development of the FAs during the course of the experiment.

The tracking algorithm is initialized with all the adhesions detected in the first frame of the image sequence. The first step of the tracking algorithm attempts to locate FAs that correspond to one another in the next time step of the experimental data (Figure S4). This first step assumes that if a focal adhesion in the first frame overlaps with a focal adhesion in the subsequent frame, these overlapping adhesions correspond to one another. When an adhesion overlaps with more than one adhesion in the following frame, the adhesion with the greatest percentage of overlap is assigned as the match. If a FA does not overlap with any of the FAs in the following image, the FA closest to that adhesion in terms of the Euclidean distance between each adhesion's centroid is assigned as a match. Adhesions in the next frame that are not selected via either of these methods, but still overlap with an adhesion in the current frame are marked as being created via a split birth event. Adhesion births that are the result of split events are dealt with in later filtering steps. All of the living focal adhesions are assigned a corresponding FA in the following image by these percentage overlap and centroid distance rules.

This process of assigning live adhesions in one frame to corresponding adhesions in the following frame produces sets of adhesions that are predicted to merge. Some of these merge

events are true merge events where one adhesion has joined with another, while others are adhesions which die, but are erroneously assigned as merge events. When a FA does not overlap with the FA it is predicted to become, this FA is assumed to have died and its lineage is ended. These adhesions are also marked as having undergone a death, which will be used in later filtering steps. For the remaining merge events where more than one adhesion has been predicted to merge in the next frame, one of the merging FA lineages is selected to continue, while the other FA lineage is predicted to end. When the adhesions predicted to merge differ in size by at least 10%, the larger adhesion's lineage is continued. If the merging FA's sizes do not differ by at least 10%, the lineage whose current centroid is closer to the adhesion centroid in the following image is predicted to continue. By this sequence of rules, each merge event is resolved so that corresponding FAs in experimental data images are determined.

After tracking live adhesions and resolving the merge and death events, the last step involves starting lineages that correspond to newly born adhesions. New lineages are started for the adhesions that had no match in the prior frame (birth events). This process of tracking the live adhesions, resolving merge and death events and starting new lineages is repeated for each image in the experimental data sequence until adhesion data from all the images have been processed.

Calculating Assembly and Disassembly Rates

With the adhesions tracked through each experiment, the static properties determined for each adhesion in each frame of the time-lapse movie are collected into a set of data time series representing the properties of each adhesion through time. One type of time series follows the mean intensity of Paxillin through time, making it possible to estimate the rates of assembly and disassembly of Paxillin for each adhesion. An automated method to estimate the rates of

assembly and disassembly was developed. This program automatically fits linear models to the log-transformed time series of Paxillin intensity values for both the assembly and disassembly phases of the FA life cycle.

In the first part of the algorithm, linear models are fit to all the possible assembly and disassembly phases greater than or equal to a user specified length. The assembly phase is assumed to occur at the beginning of the time series, whereas the disassembly phase is assumed to end with the last point in the time series (FA death). Each of the fits collected were normalized by either the first (assembly rate calculations) or last point (disassembly rate calculations) in the time series and log-transformed, as described [7].

In the second part of the algorithm, the optimum lengths of the assembly and disassembly phases were determined via a search for the maximum sum of adjusted R^2 values of the model fits. It was assumed that the assembly and disassembly phases did not overlap. In the rare cases where there are multiple combinations of assembly and disassembly times that produce the highest sum of adjusted R^2 values, the combination with the longest combined assembly and disassembly times is selected. The stability/maturity period was then defined as the length of time between the assembly and disassembly periods.

Results Filtering

Several filters are used to analyze the data sets collected with these analysis methods. When determining the assembly and disassembly rates, only adhesions with at least 20 Paxillin intensity time points were analyzed. This ensured that there was sufficient data available to correctly detect the assembly and disassembly rates. Adhesions whose birth was the result of a split event were also excluded from the assembly rate calculations, while adhesions whose

lineage ended with a merge event were excluded from the disassembly rate calculation. Assembly and disassembly fits whose linear model p-values were above 0.05, indicating that the slope of the linear model was not significantly different from zero, were also excluded from the data set.

A separate set of filters was used to determine the length of each phase (assembly, stability and disassembly) in the adhesion intensity time series data. In order to estimate the length of time an adhesion spends in the stability phase, we required that both the assembly and disassembly phases be observed. In addition, the adhesion birth could not have been the result of a split event and the death of the adhesion not the result of a merge. The filter also excluded those adhesions where the p-value of either the assembly or disassembly linear model was greater than 0.05.

Parameter Testing

To test the sensitivity of results on parameters used for defining the threshold for adhesion detection, the minimum length of the assembly and disassembly phases and the rate of image sampling, we re-executed our analysis while varying these parameters. The threshold for adhesion detection was varied between 0.05 and 0.10, with no significant effect on the percentage change between the wild-type cells and the S178A mutant cells in either the assembly or disassembly rates (Figure S5 and Figure S6). Varying the required length for assembly and disassembly rate calculation similarly had no significant effect on percentage change between the wild-type and S178A mutant cells of the rates of assembly or disassembly (Figure S7 and Figure S8). Finally, we tested the results of changing the image sampling rate by discarding every other collected image in the same set of experiments (Figure S9). Discarding half of the images did not

significantly affect the assembly or disassembly rates, but did have a slight effect on the distribution of the adjusted R^2 values (Figure S10).

Software Testing

In order to test the baseline performance of the algorithms, a set of gold standard images were produced with sets of FAs having specific, predefined properties. In general, validation tests consisted of simulating a time-lapse microscope field of view that mimicked the observed properties of the adhesions (Figure S11A). Since our results are consistent with prior findings based on manual methods of adhesion identification, the simulated range of properties was set to be similar to those observed in the experimental data. For all simulated experiments, a Gaussian noise model (mean 0, variance of $2*10^{-3}$) was used as a background to simulate the cell environment. These parameters were chosen as they produced distributions of short-lived adhesions that were empirically similar to those observed experimentally. Also, all simulated adhesions were circular and the same background noise model was used to perturb intensities assigned by the software to each simulated adhesion.

Three types of simulations were conducted: stationary, moving and kinetic. The stationary simulation consisted of simulating a field of view that included rows and columns of unmoving adhesions. The intensity of the adhesions were varied along the columns between mean intensities of 0.05 and 0.47 (95% of the detected adhesions in the experimental data fall between normalized average Paxillin intensities of 0.21 and 0.52). Ten different adhesion radii were simulated along the rows, varying between 0.5 and 5 pixels. The adhesions at low mean intensity values were not reliably discernable below intensity level 0.17. Adhesions above this level were readily detected with both the predicted intensities and sizes (Figure S11).

The moving simulation was designed to probe the tracking algorithm's performance in

following adhesions of various sizes and intensities. The simulation consisted of sliding the adhesions across the field of view at different rates (Figure S12A). As expected, the smaller adhesions were more difficult to track, with a nearly linear relationship between the ability to track an adhesion moving at a certain rate and its corresponding radius (Figure S12B). As long as the adhesion is detectable, there does not appear to be any differences in the intensity versus tracking accuracy (data not shown).

To conduct the adhesion kinetics tests, sets of adhesions were simulated that went through logarithmic assembly and disassembly phases. The assembly and disassembly rates were varied by shortening or lengthening the amount of time each adhesion spent reaching maximum intensity. The stability period in each of these adhesions was set to five frames. Assembly and disassembly lengths between 10 and 20 were all tested. In order to avoid biasing the automated assembly and disassembly phase fitting software to higher phase lengths, the minimum phase length was set to five time points during image analysis. Overall, the software was able to reliably extract both the expected assembly and disassembly rates and length of time spent in each phase (Figure S13). There were several samples in the longer phase lengths that were predicted to have substantially shorter assembly and disassembly phase lengths than that specified by the software, but these simulated adhesions were in the minority and did not significantly affect the confidence intervals around the mean assembly and disassembly lengths. These simulations further support the accuracy of results derived from applying the same sets of algorithms to the analysis of adhesions in living cells.

Statistical Tests

Two different types of tests were used to determine the statistical significance of the differences between the adhesions in the wild-type, S178A and labeled-FAK adhesions. To

compare datasets with <2000 points, bootstrap resampling was used to determine either the mean or median distribution. From these distributions the p-value was determined using the percentile method. The bootstrap method was too computationally intense to compare datasets, such as the area and axial ratio of the adhesions, with significantly more points than 2000 data points. Instead, the Wilcox Rank Sum test was used to find the p-value in these cases.

Software Availability

The most recent version of the software system is available from the Gomez lab website (http://gomezlab.bme.unc.edu/tools). In addition to the source code, released under the BSD license, there is a sample movie that can be used to test the success of installing the analysis system. The software has been tested on Mac OS X 10.5 and Ubuntu Linux 10.04.

Acknowledgements

This work was supported by NIH grants GM57464,P01 HL080166 (KMH), and F31 NS062487 (EAV), startup funds from the UNC School of Medicine (SMG) and the NSF Graduate Research Fellowship Program (MEB). The authors would like to thank members of the Gomez lab for critical reading of early drafts of the manuscript, members of the Jacobson, Bear, and Hahn labs at UNC-CH for providing the retroviral vectors used in this study, and UNC Research Computing for access to computational resources.

REFERENCES

1. Geiger B, Spatz JP, Bershadsky AD (2009) Environmental sensing through focal adhesions. Nat Rev Mol Cell Biol 10: 21-33.

2. Lauffenburger DA, Horwitz AF (1996) Cell migration: a physically integrated molecular process. Cell 84.

3. Ridley AJ, Schwartz MA, Burridge K, Firtel RA, Ginsberg MH, et al. (2003) Cell Migration: Integrating Signals from Front to Back. Science 302.

4. Larsen M, Tremblay ML, Yamada KM (2003) Phosphatases in cell-matrix adhesion and migration. Nat Rev Mol Cell Biol 4: 700-711.

5. Webb DJ, Parsons JT, Horwitz AF (2002) Adhesion assembly, disassembly and turnover in migrating cells - over and over and over again. Nat Cell Biol 4.

6. Ballestrem C, Hinz B, Imhof BA, Wehrle-Haller B (2001) Marching at the front and dragging behind: differential alphaVbeta3-integrin turnover regulates focal adhesion behavior. J Cell Biol 155: 1319-1332.

7. Webb DJ, Donais K, Whitmore LA, Thomas SM, Turner CE, et al. (2004) FAK--Src signalling through paxillin, ERK and MLCK regulates adhesion disassembly. Nature Cell Biology 6.

8. Nayal A, Webb DJ, Brown CM, Schaefer EM, Vicente-Manzanares M, et al. (2006) Paxillin phosphorylation at Ser273 localizes a GIT1-PIX-PAK complex and regulates adhesion and protrusion dynamics. The Journal of Cell Biology 173.

9. Bryce NS, Clark ES, Leysath JL, Currie JD, Webb DJ, et al. (2005) Cortactin promotes cell motility by enhancing lamellipodial persistence. Curr Biol 15: 1276-1285.

10. Owen KA, Pixley FJ, Thomas KS, Vicente-Manzanares M, Ray BJ, et al. (2007) Regulation of lamellipodial persistence, adhesion turnover, and motility in macrophages focal adhesion kinase. J Cell Biol.

11. Kobayashi T, Hino S-i, Oue N, Asahara T, Zollo M, et al. (2006) Glycogen Synthase Kinase 3 and h-prune Regulate Cell Migration Modulating Focal Adhesions. Mol Cell Biol 26.

12. Franco SJ, Rodgers MA, Perrin BJ, Han J, Bennin DA, et al. (2004) Calpain-mediated proteolysis of talin regulates adhesion dynamics. Nat Cell Biol 6.

13. Paran Y, Ilan M, Kashman Y, Goldstein S, Liron Y, et al. (2007) High-throughput screening of cellular features using high-resolution light-microscopy; Application for profiling drug effects on cell adhesion. Journal of Structural Biology 158.

14. Zamir E, Geiger B, Kam Z (2008) Quantitative Multicolor Compositional Imaging Resolves Molecular Domains in Cell-Matrix Adhesions. PLoS ONE 3: e1901.

15. Winograd-Katz SE, Itzkovitz S, Kam Z, Geiger B (2009) Multiparametric analysis of focal adhesion formation RNAi-mediated gene knockdown. J Cell Biol 186.

16. Brown MC, Turner CE (2004) Paxillin: Adapting to Change. Physiological Reviews 84.

17. Huang C, Rajfur Z, Borchers C, Schaller MD, Jacobson K (2003) JNK phosphorylates paxillin and regulates cell migration. Nature 424.

18. Kimura K, Teranishi S, Yamauchi J, Nishida T (2008) Role of JNK-Dependent Serine Phosphorylation of Paxillin in Migration of Corneal Epithelial Cells during Wound Closure. Investigative Ophthalmology Visual Science 49.
19. Huang Z, Yan D-P, Ge B-X (2008) JNK regulates cell migration through promotion of tyrosine phosphorylation of paxillin. Cellular Signalling 20.
20. Vallotton P, Gupton SL, Waterman-Storer CM, Danuser G (2004) Simultaneous mapping of filamentous actin flow and turnover in migrating cells quantitative fluorescent speckle microscopy. PNAS 101.
21. Machacek M, Hodgson L, Welch C, Elliott H, Pertz O, et al. (2009) Coordination of Rho GTPase activities during cell protrusion. Nature 461: 99-103.
22. Zamir E, Katz BZ, Aota S, Yamada KM, Geiger B, et al. (1999) Molecular diversity of cell-matrix adhesions. J Cell Sci 112.
23. Machacek M, Danuser G (2006) Morphodynamic Profiling of Protrusion Phenotypes. Biophys J 90.

Figure Captions

Figure 1. Automating the analysis of focal adhesion images requires a multi-stage pipeline. The first row shows several representative images of fluorescently labeled Paxillin using TIRF microscopy. In the second row, a cartoon depiction of the segmented adhesions and the cell edge are shown. Identification of the adhesions in each image allows a set of static morphological and fluorescence intensity-based features to be extracted. The third row shows a single adhesion (highlighted in red) being tracked through the short sample time course. The properties of each adhesion are tracked over time, allowing the large scale dynamics of FA to be determined.

Figure 2. Applying quantitative image processing methods to FA images allows comprehensive characterization of FA properties. (A) One frame from a 200 minute movie of NIH 3T3 cells expressing GFP-Paxillin (the scale bar represents 10μm). (B) The same cell as in (A), with each adhesion outlined in a different color. (C) The entire set of adhesions in an experiment can be visualized by overlaying the adhesions from each microscopy image using a

different color for the set of adhesions at each time point. This example includes the adhesions from 198 images. (D) A large range of properties can be extracted from the segmented FA. Five samples are provided. The area histogram was filtered to only include adhesions with areas less than 5μm^2. The axial ratio histogram was filtered to only include adhesions with an axial ratio of 8 or less. The longevity histogram includes all adhesions, while the inset only includes adhesions with longevity greater than 20. The histograms include data from 21 cells.

Figure 3. Automated measurement of focal adhesion dynamics. (A) Each of the adhesions in the cells is tracked, allowing the position and properties of single adhesions and populations to be assessed. Here a single adhesion (in green), the surrounding adhesions (in blue) and the cell edge (in red) are followed for 49 minutes. The cell edge is only outlined in the first frame. The scale bar is 10μm. (B) The intensity of EGFP- Paxillin in the tracked adhesion in (A) through time. The green, yellow and red lines are smoothed using the Lowess algorithm and correspond to the assembly, stable and disassembly phases, respectively. (C) The normalized log-linear fit of the Paxillin intensity through time during the assembly phase of the adhesion in part (B). The inset depicts several of the images from which the Paxillin intensity was gathered. (D) The normalized log-linear fit of the Paxillin intensity through time during the disassembly phase of the adhesion in part (B). (E) The assembly and disassembly rates for adhesions whose Paxillin intensity curve fits have R^2 values of 0.9 or greater. The top and bottom lines of the boxes indicate the 3rd and 1st quartiles respectively, while the bold central lines indicate the median values. The whiskers extend up to 1.5 times the interquartile range.

Figure 4. Spatial properties of FA positions at birth and death. (A) The majority of adhesions are born within 5μm of the cell edge and the greatest variance in assembly rates are also observed in this 5μm band. (B) The distribution of the distance of death location from the cell edge indicates that adhesion disassembly typically occurs along a broader band from the cell edge as compared to the position at adhesion birth. Also, the variance in disassembly rate is roughly the same regardless of the position at adhesion death.

Figure 5. The assembly and disassembly rates of EGFP-Paxillin and EGFP-FAK adhesions are the same. The blue numbers in each plot are the p-values of the difference in median values between the EGFP-Paxillin and EGFP-FAK adhesions. P-values were calculated using the bootstrapped confidence intervals with 50000 replicates. Data from 10 cells is included in the FAK data set.

Figure 6. The S178A mutation in Paxillin decreases adhesion size and axial ratio. There are 44685 adhesions in the wild-type and 73305 adhesions in the S178A data sets. The p-values were calculated using the Wilcox Rank Sum test. Data from 9 cells is included in the S178A data set.

Figure 7. The S178A mutation in Paxillin alters adhesion assembly and disassembly. (A and B) The rate of adhesion assembly and disassembly are significantly decreased by the S178A mutation. The S178A median FA assembly rate is decreased by 42% compared to the wild-type cells, while the median disassembly rate is decreased by 36%. (C and D) The S178A mutation shifts the median adhesion birth location away from the cell edge, but has no effect on the location of cell death. The S178A median adhesion birth position is 31% greater than wild-type

median birth position. The median position at adhesion death is decreased by 4% between the S178A and wild-type cells. P-values were calculated in the same manner as in Figure 5.

Figure 8. The lengths of the assembly and disassembly phases in S178A mutant FAs are significantly different from those in the wild-type, while the stability phase lengths are unaffected. The phase length values include all adhesions where the log-linear models fit with a p-value of 0.05 or less. Error bars indicate 99% confidence intervals on the mean phase length as determined through 50,000 bootstrap samples. A double asterisk (**) indicates $p<10^{-5}$ and single asterisk (*) indicates $p<0.05$. Wild-type N Values: Assembly (1068), Stability (465), Disassembly (1392); S178A N Values: Assembly (2106), Stability (870), Disassembly (1802).

Figure 9. Summary of results and conceptual model of how the S178A mutant affects the adhesion life cycle. Durations and slopes are shown to scale.

Figure S**1**. The assembly and disassembly log-linear models fit the Paxillin intensity time courses with high R^2 values. **The red lines indicate the median length-adjusted R^2 values.**

Figure S2. Adhesions labeled with EGFP-FAK are larger in mean area and have a larger axial ratio than those labeled EGFP-Paxillin. There are 51836 adhesions in the FAK data set and 44685 adhesions in the Paxillin data set. The p-values were calculated using the same methods as Figure 6.

Figure S3. There were not any significant differences between the expression levels in the EGFP-Paxillin and EGFP-PaxillinS178A cell lines. The average intensity of fluorescence

inside the cell is shown in three different ways: the overall cell intensity (A), inside the cell not including the adhesions (B) and only the adhesions (C). The error bars are 95% confidence intervals determined using 50,000 bootstrap samples on the mean value. There are 21 cells in the wild-type and 9 cells in the S178A data sets.

Figure S4. Flow chart for the tracking software adhesion following algorithm.

Figure S5. Changing the adhesion detection threshold does not affect the differences in the assembly rates between S178A mutant and wild-type cells. Each boxplot contains all the adhesions with significant linear fits (linear model p-value below 0.05). The p-values in each boxplot are for the difference in medians between the wild-type and S178A data sets in each boxplot.

Figure S6. Changing the adhesion detection threshold does not affect the differences in the disassembly rates between S178A mutant and wild-type cells. Each boxplot contains all the adhesions with significant linear fits (linear model p-value below 0.05). The p-values in each boxplot are for the difference in medians between the wild-type and S178A data sets in each boxplot.

Figure S7. Changing the minimum length of the assembly phase does not significantly affect the differences in the assembly rate between the wild-type and S178A mutant cells. Each boxplot contains all the adhesions with significant linear fits (linear model p-value below 0.05). The p-values in each boxplot are for the difference in medians between the wild-type and S178A data sets in each boxplot.

Figure S8. Changing the minimum length of the disassembly phase does not significantly affect the differences in the assembly rate between the wild-type and S178A mutant cells. Each boxplot contains all the adhesions with significant linear fits (linear model p-value below 0.05). The 95% confidence intervals on the percent change in the median assembly rate between the wild-type and S178A adhesions overlap in all minimum length settings. The p-values in each boxplot are for the difference in medians between the wild-type and S178A data sets in each boxplot.

Figure S9. Reducing the time between each frame only has mild effects on the assembly and disassembly rates in the wild-type cells. The label 'All' indicates that none of the images were excluded to estimate the rates, while 'Sampled' indicates that every other image from each experiment was discarded. To compensate for the shortened experimental time, the minimum number of points needed to determine an assembly or disassembly rate was reduced to 5 for the sampled data sets. Each boxplot describes the data from all the adhesions with significant linear fits (p-value below 0.05).

Figure S10. Reducing the time between each frame only has mild effects on the assembly and disassembly rates in the S178A cells. The label 'All' indicates that none of the images were excluded to estimate the rates, while 'Sampled' indicates that every other image from each experiment was discarded. To compensate for the shortened experimental time, the minimum number of points needed to determine an assembly or disassembly rate was reduced to 5 for the sampled data sets. Each boxplot describes the data from all the adhesions with significant linear fits (p-value below 0.05).

Figure S11. Evaluation of the analysis system's ability to extract quantitative properties from simulated stationary focal adhesions. (A) The last frame of the stationary simulation, with each adhesion outlined in a color depending on when in the movie it was born. The adhesions in blue have been detected for the longest time, while those in red and orange have been detected for the shortest amount of time. The simulated adhesions in columns 1-3 are all too faint to be reliably detected for the length of the simulation experiment, while those in column 4 are near the limit of detection. (B) The exponential distribution of adhesion longevity appears similar to that observed in the experimental data. The longevity of all the detected adhesions was correctly identified as 25 minutes. (C and D) The average adhesion intensity (C) and mean adhesion area (D) were correctly identified in the adhesions that were detected for their entire 25 minute lifespan. The red lines in C indicate the true values.

Figure S12. Evaluation of the tracking algorithm's ability to follow adhesions of various sizes and speeds. (A) A sample frame from the simulated adhesion motion experiment where the adhesions were moved at 1 pixel per frame. The top row of adhesions of only a single pixel could not be followed. (B) As the movement speed of the simulated adhesions increases, only larger adhesions can be reliably tracked.

Figure S13. Evaluation of the rate and phase length detection algorithm using simulated focal adhesion images. (A and C) The predicted median assembly (A) and disassembly (C) rates were extracted correctly by the algorithm. (B and D) The predicted lengths of both the assembly (B) and disassembly (D) were also correctly identified by the algorithm. All the red lines indicate the expected values of the properties in each plot.

Video S1. Example movie showing the results of tracking the EGFP-Paxillin labeled adhesions. The left panel shows the normalized raw experimental data, while the right hand side shows each adhesion outlined in a different color. As the movie plays, the highlighting color remains the same for each unique adhesion. The scale bar is 10μm.

Video S2. Example movie showing the results of tracking the EGFP-PaxillinS178A labeled adhesions. The left and right panels are the same as in Video S1. The scale bar is 10 μm.

Video S3. Example movie showing the results of tracking the EGFP-FAK labeled adhesions. The left and right panels are the same as in Video S1. The scale bar is 10 μm.

Figure 1. Analysis System

Click here to download high resolution image

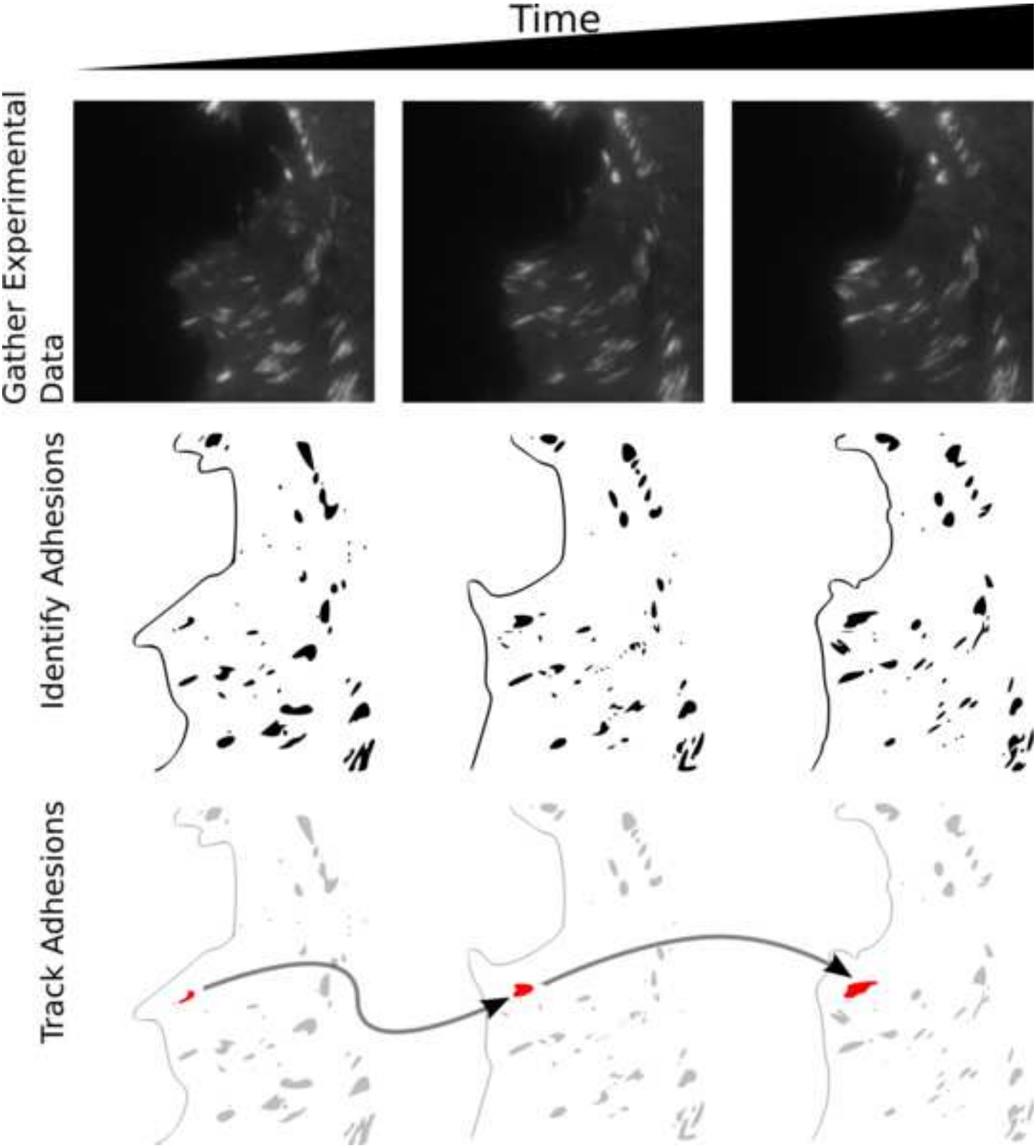

Figure 2. Statics

Click here to download high resolution image

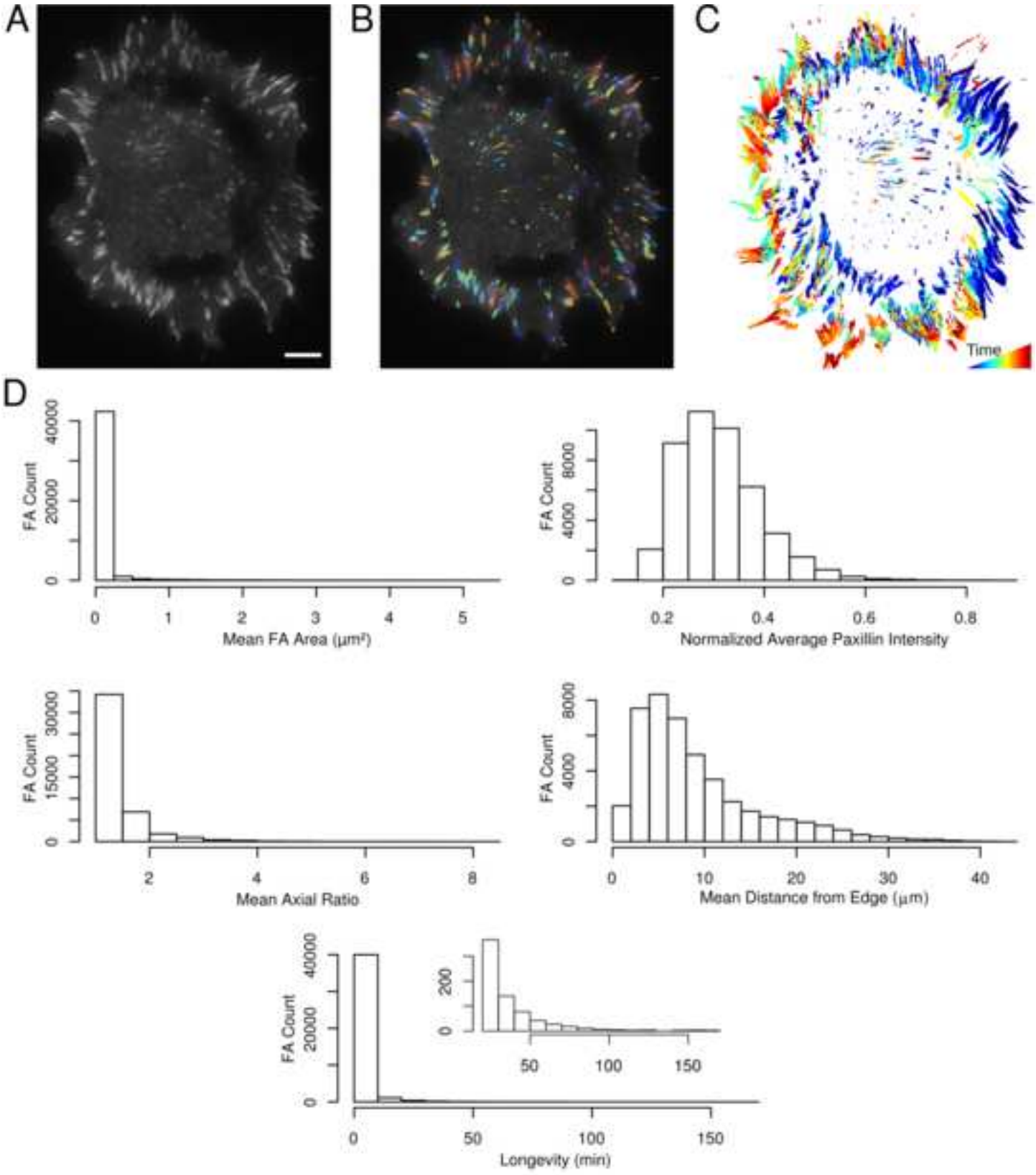

Figure 3. Kinetics

Click here to download high resolution image

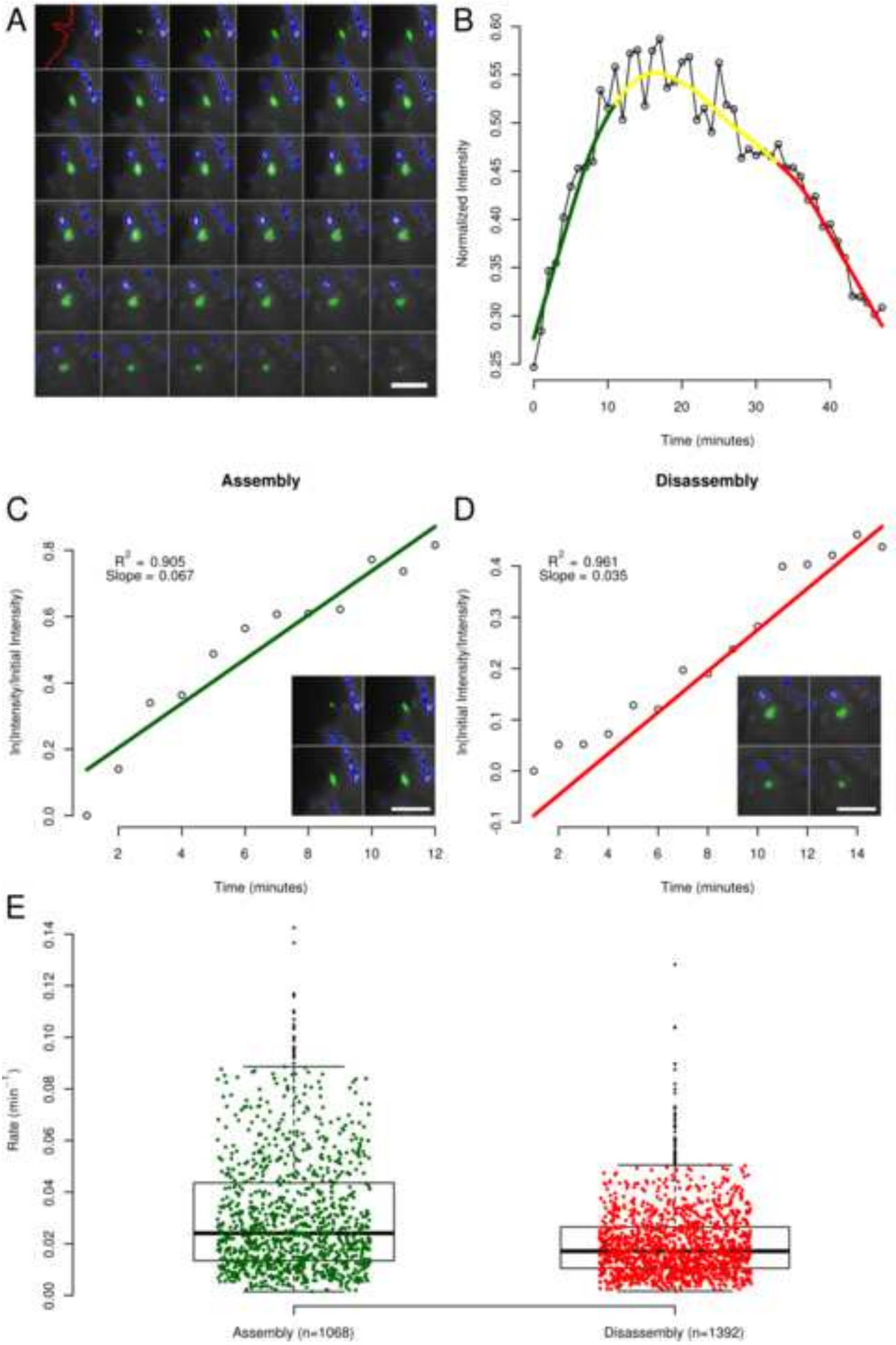

Figure 4. Spatial

Click here to download high resolution image

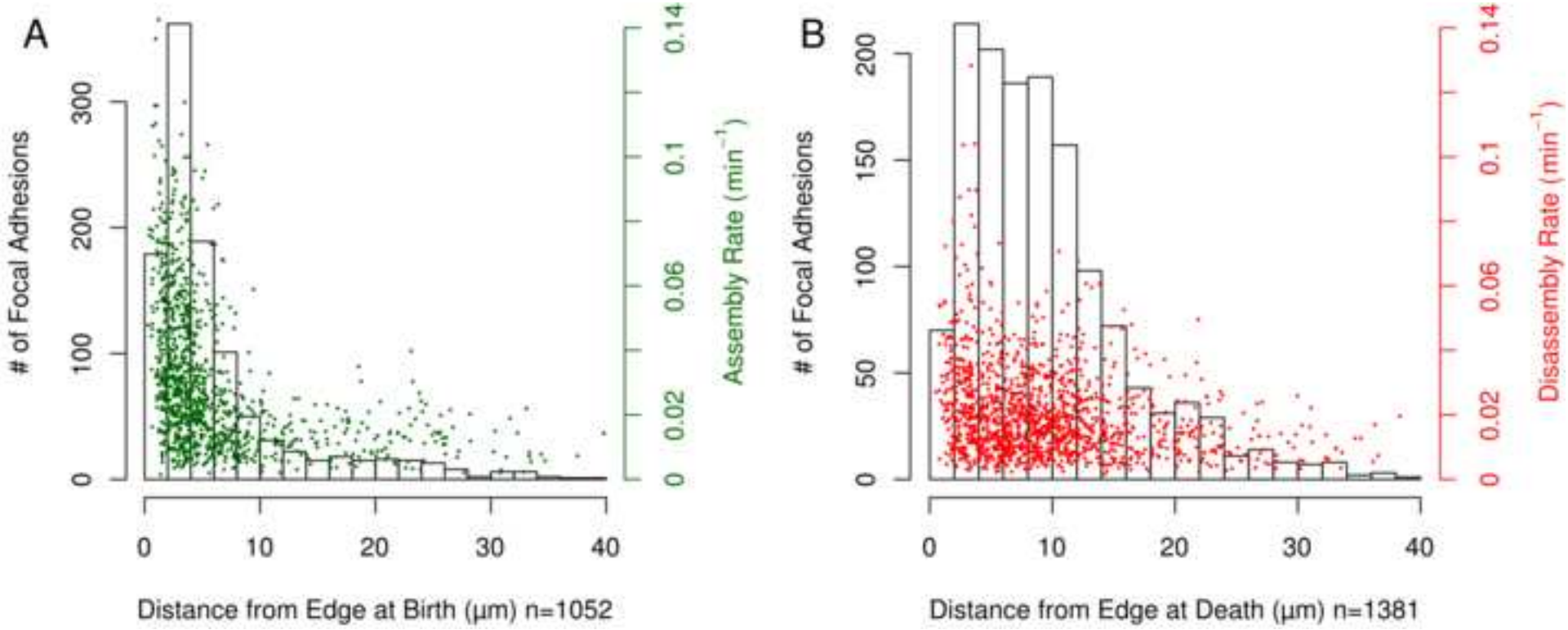

Figure 5. FAK vs Paxillin Dynamics
Click here to download high resolution image

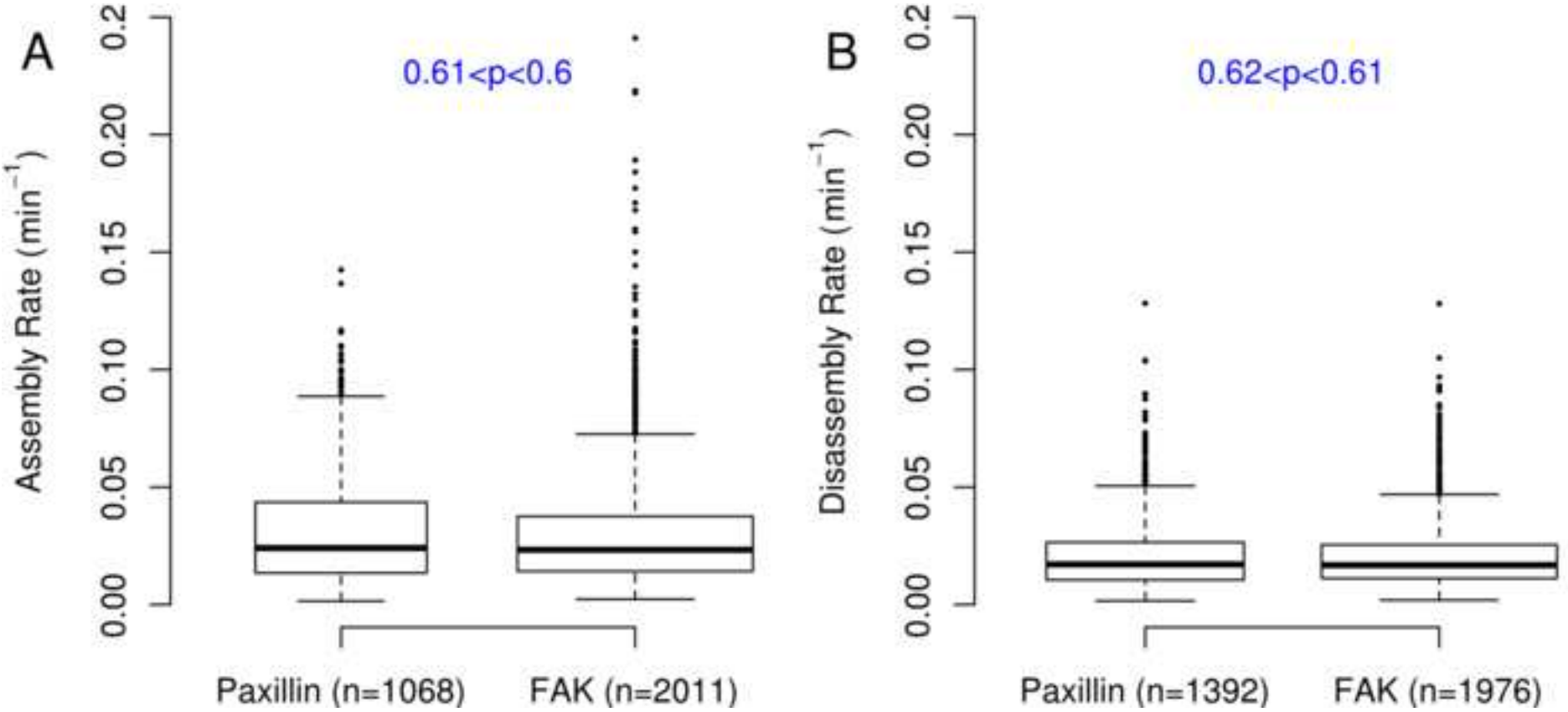

Figure 6. S718A vs Wild-type Statics
Click here to download high resolution image

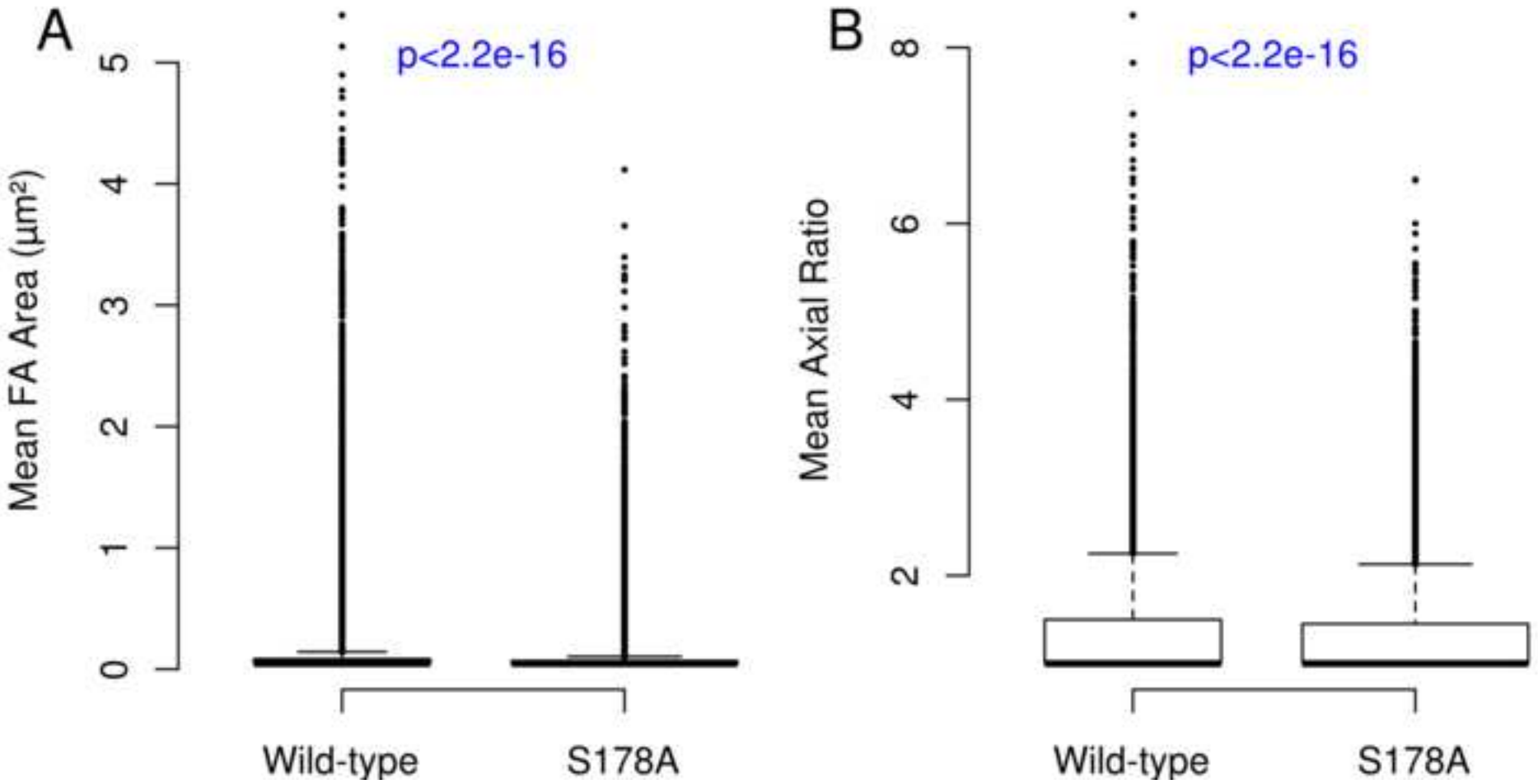

Figure 7. S718A vs Wild-type Kinetics
Click here to download high resolution image

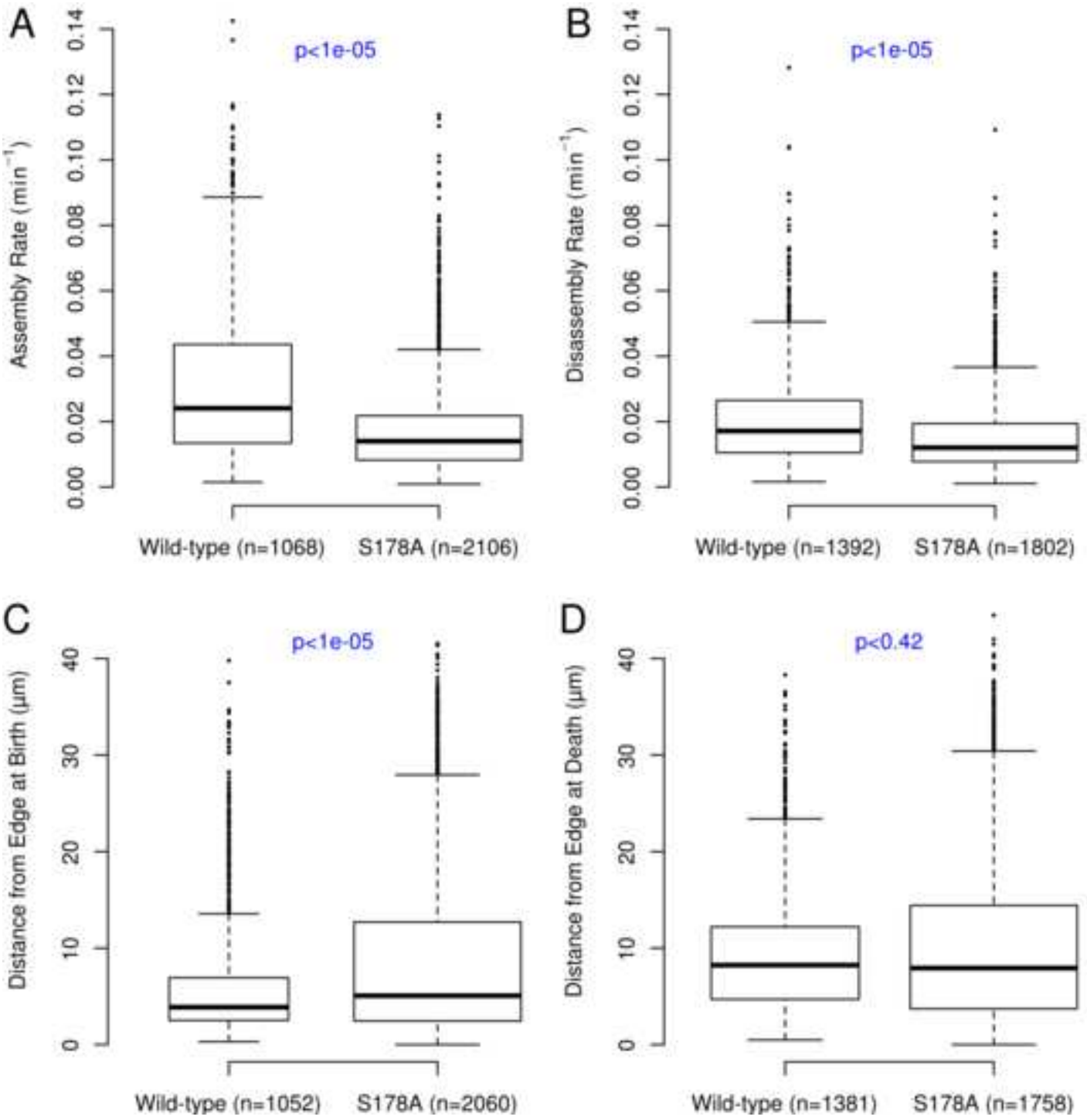

Figure 8. S178A and WT Lifetimes
Click here to download high resolution image

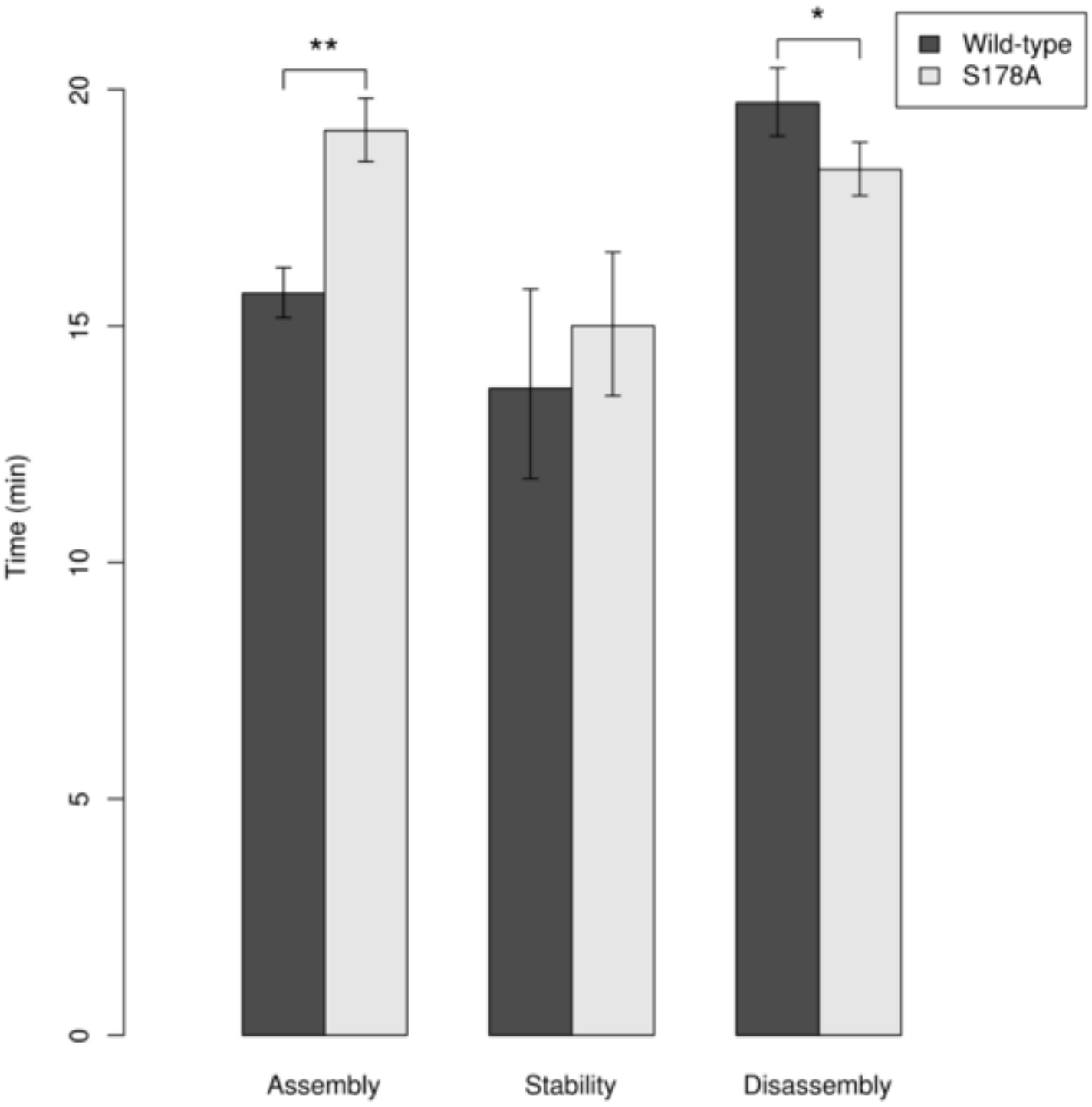

Figure 9. Conceptual Model

Click here to download high resolution image

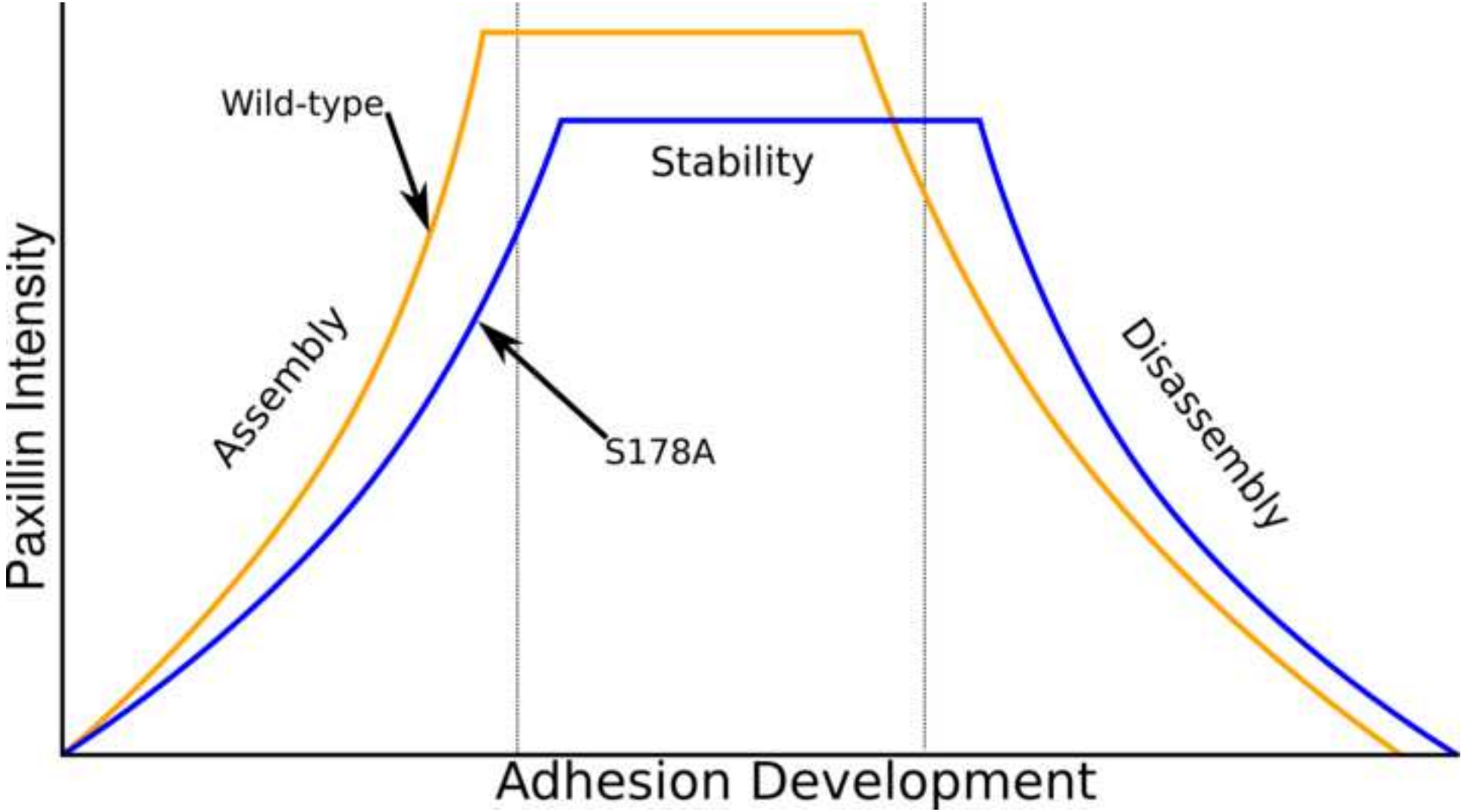

Figure S1. R-squared scores

Click here to download high resolution image

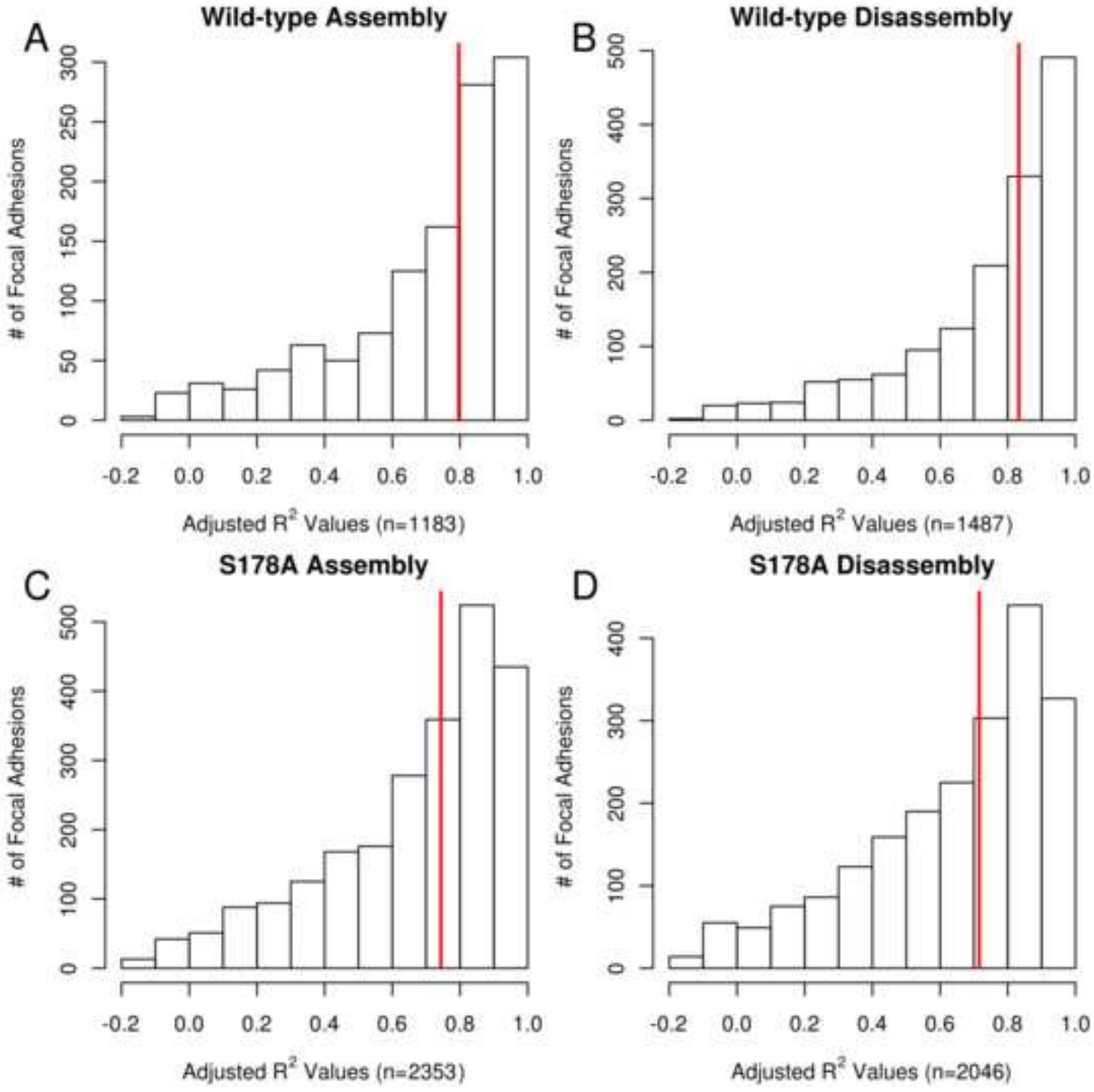

Figure S2. FAK vs Paxillin Statics
Click here to download high resolution image

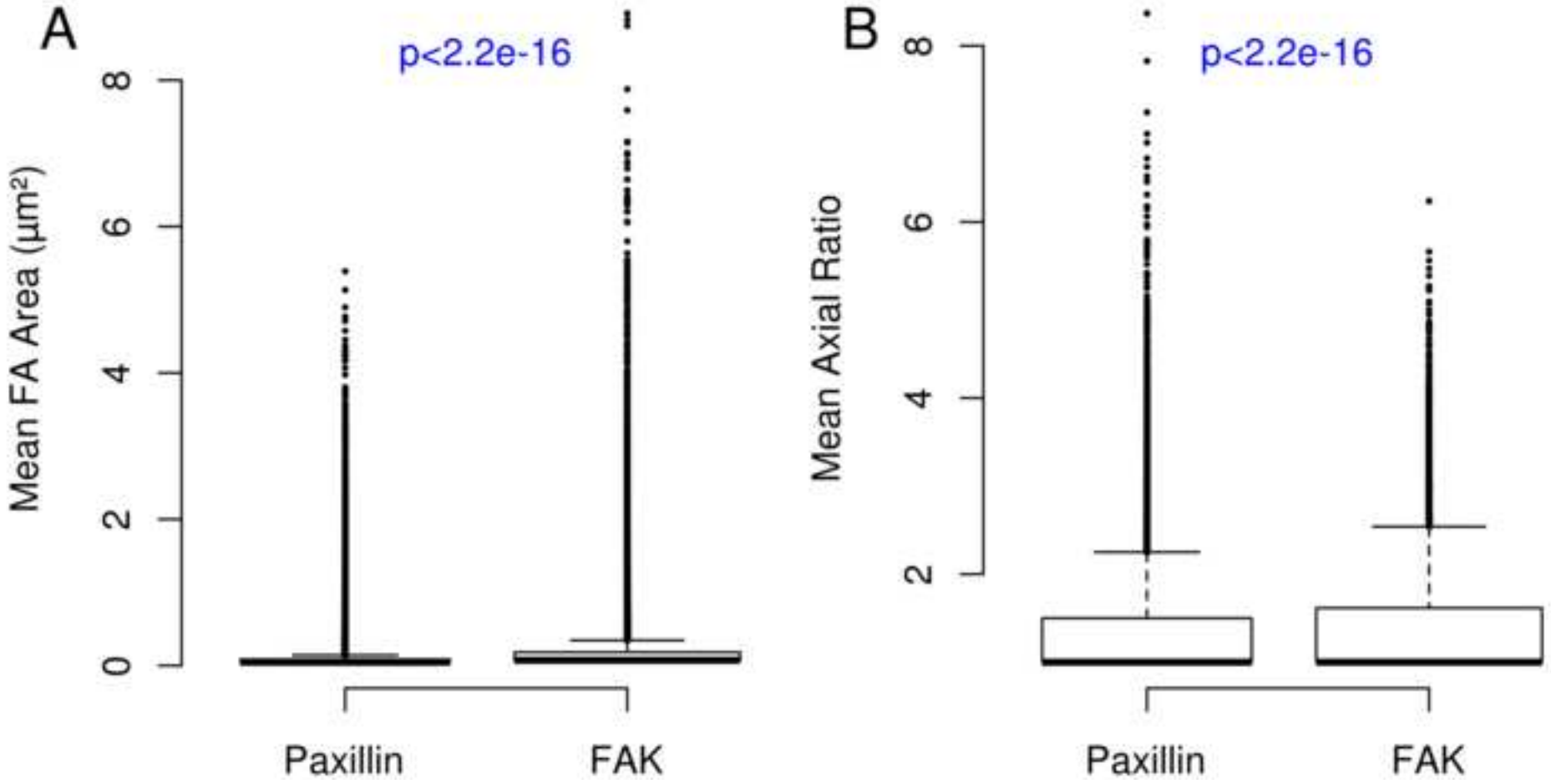

Figure S3. Expression Levels

Click here to download high resolution image

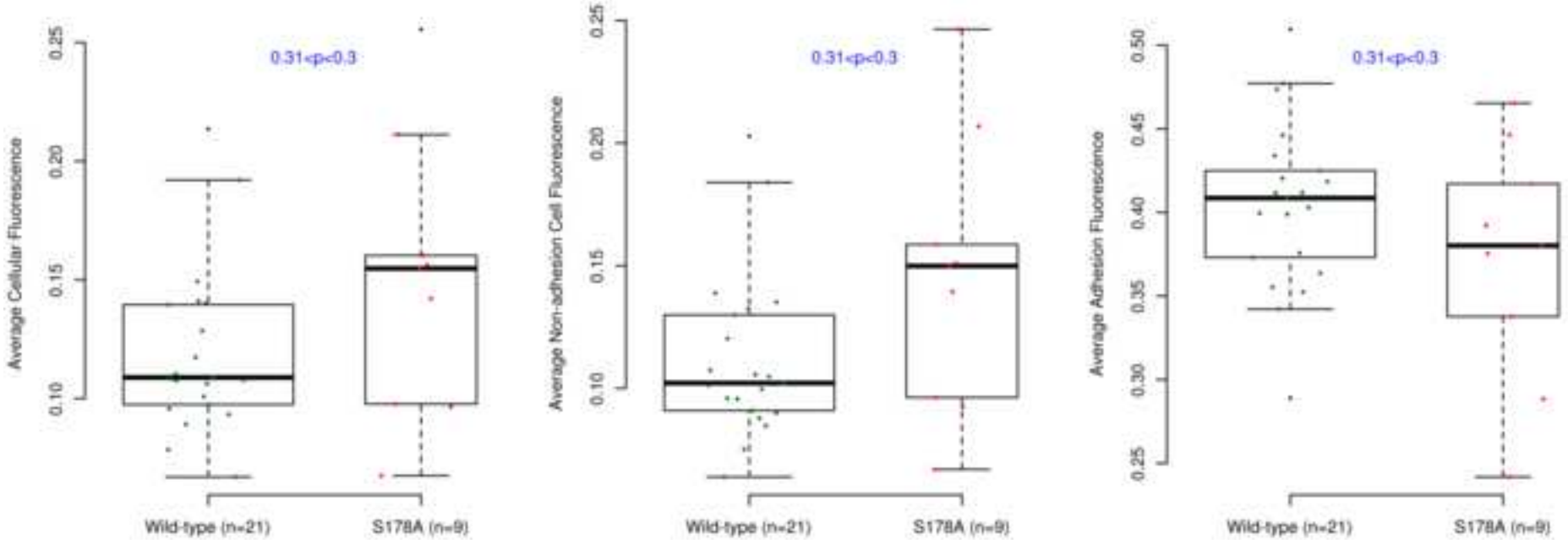

Figure S4. Tracking Flowchart
Click here to download high resolution image

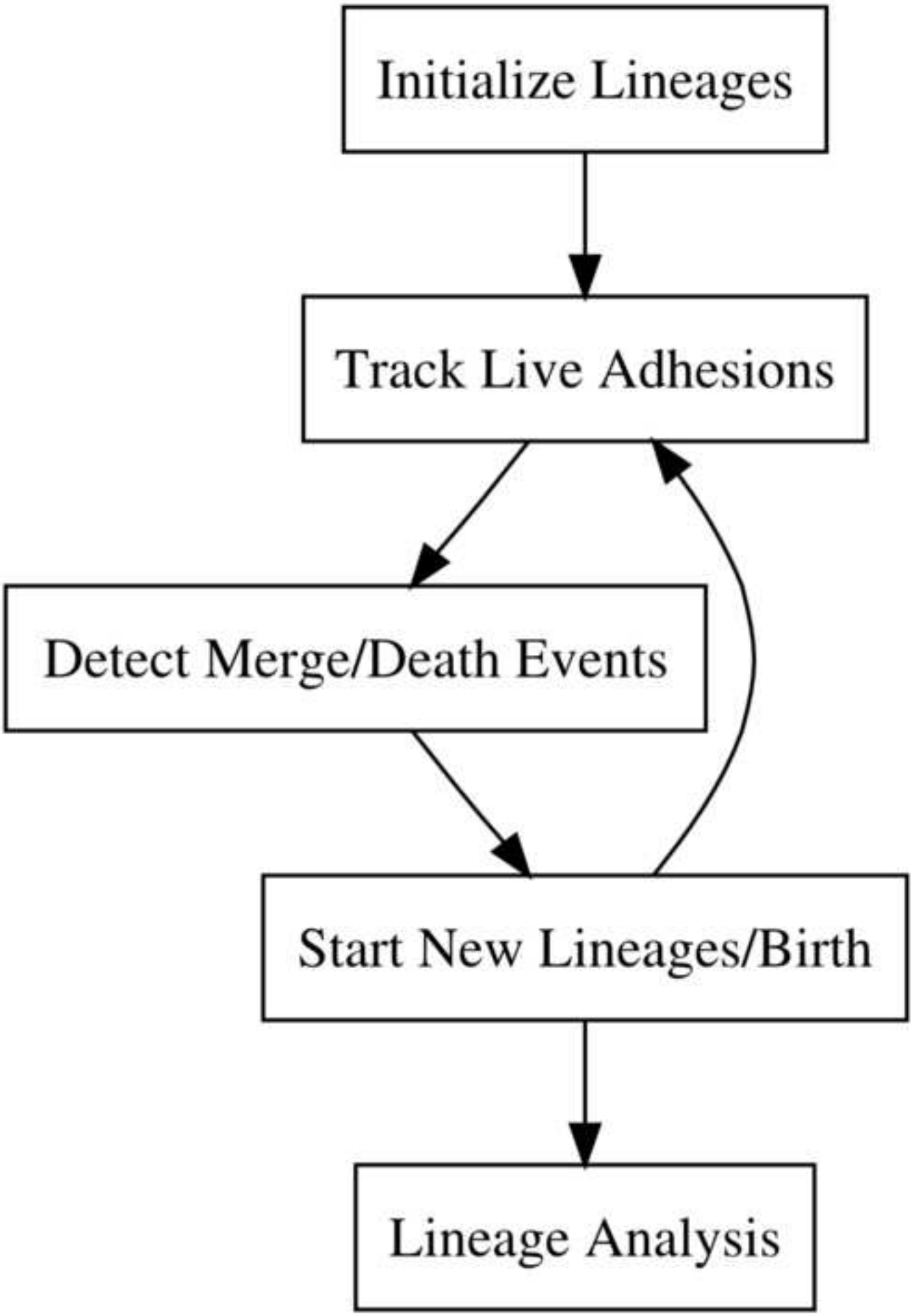

Figure S5. Threshold Variation - Assembly
Click here to download high resolution image

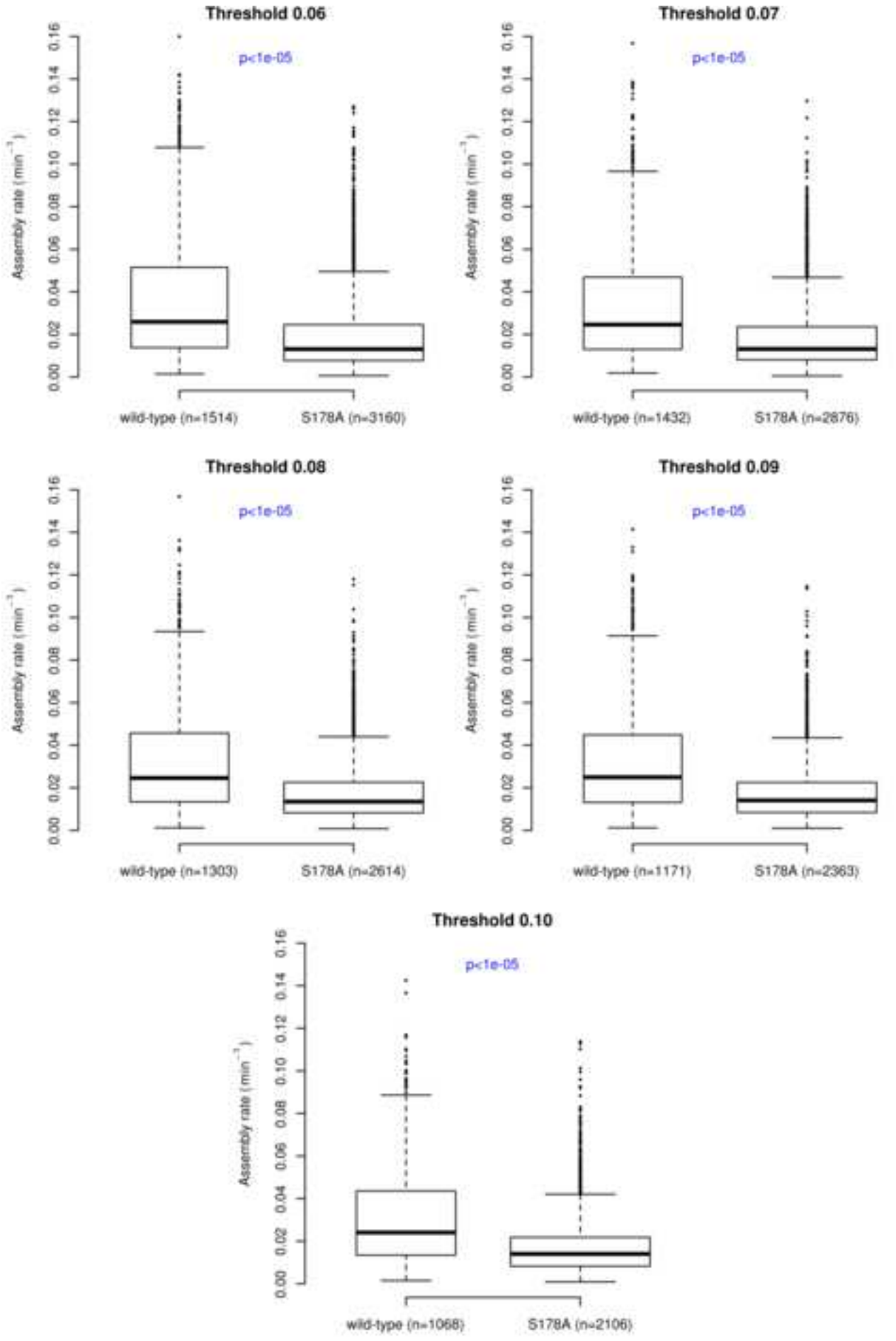

Figure S6. Threshold Variation - Disassembly
Click here to download high resolution image

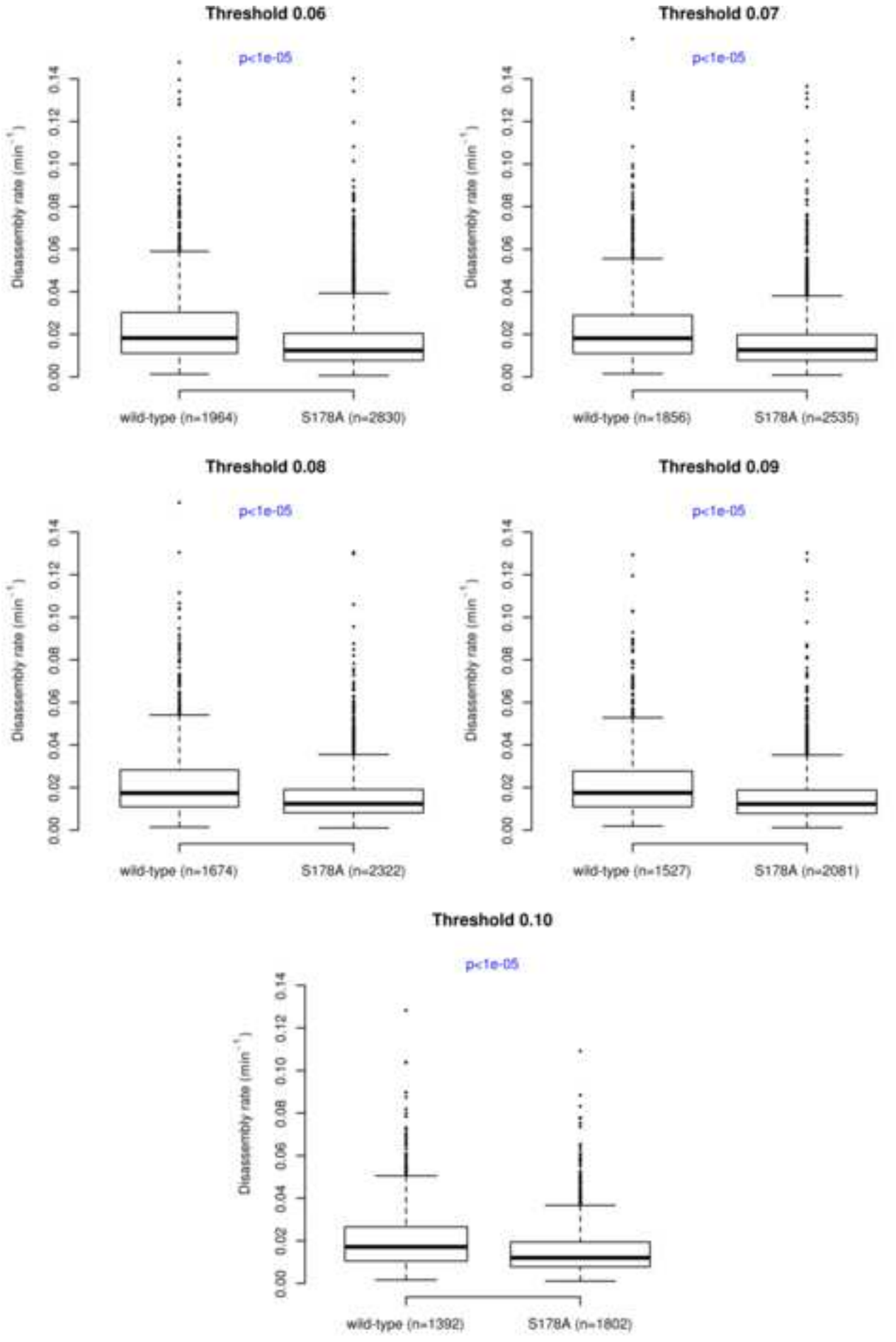

Figure S7. Phase Length - Assembly
Click here to download high resolution image

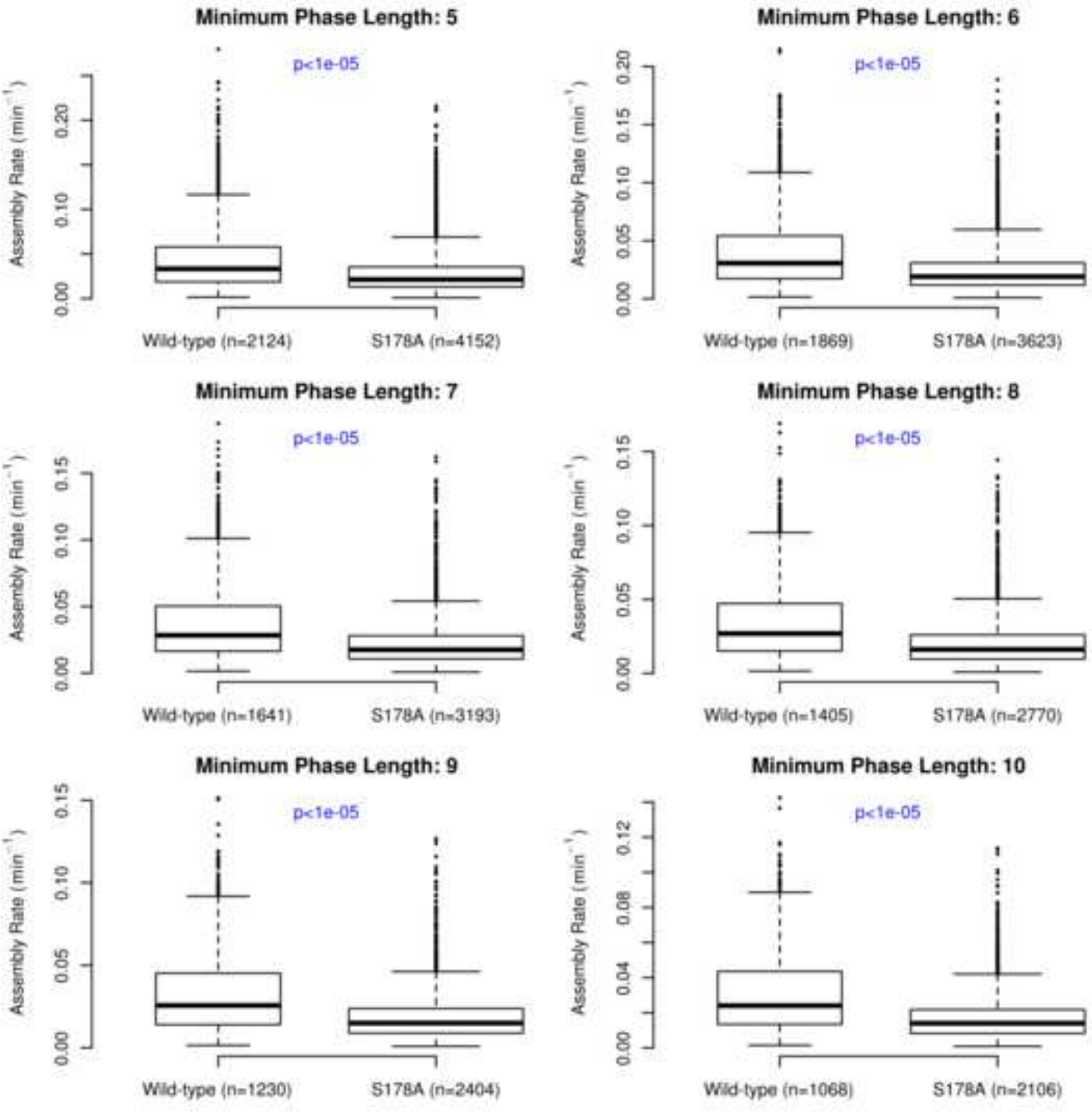

Figure S8. Phase Length - Disassembly
Click here to download high resolution image

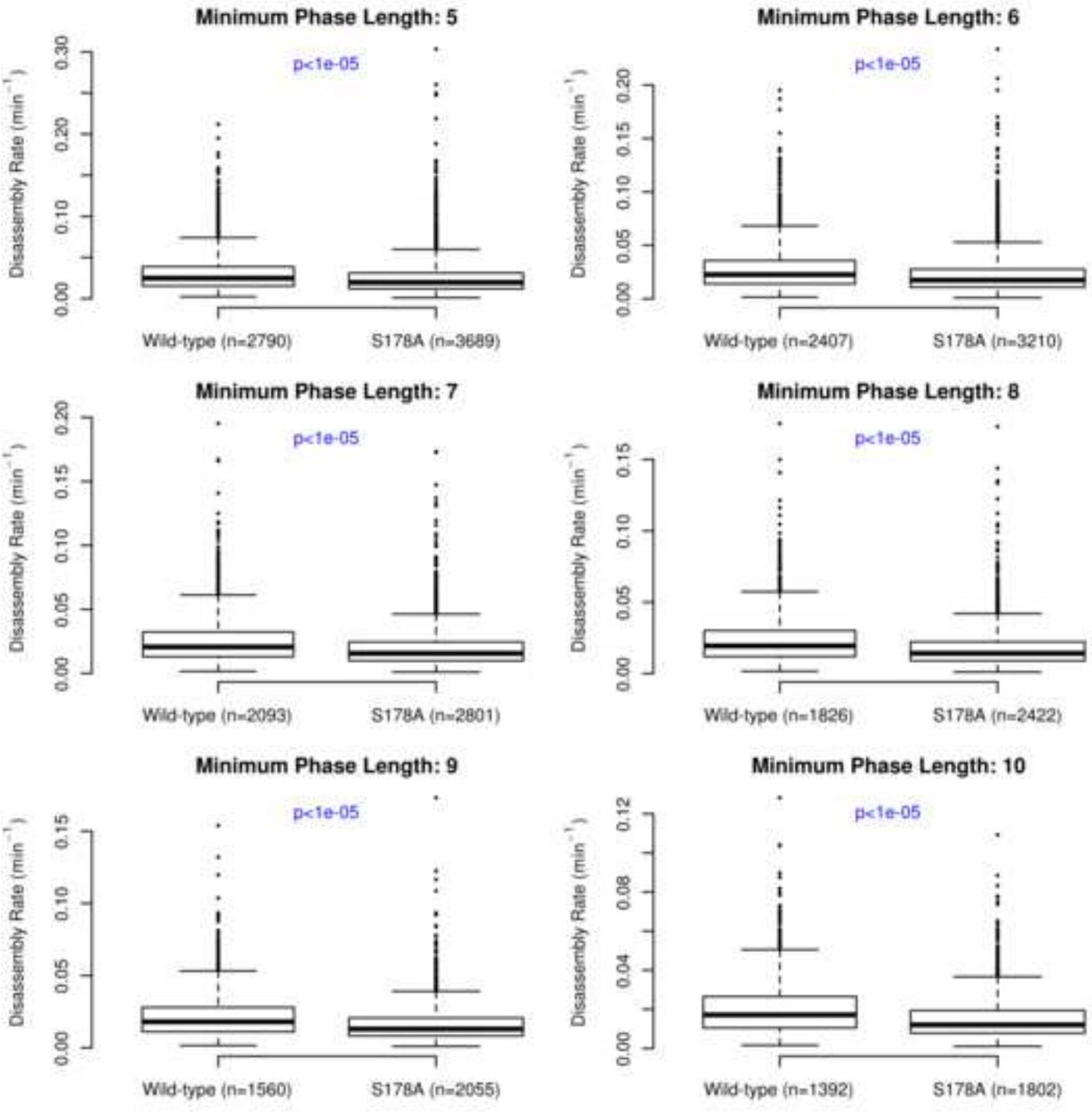

Figure S9. Sampled Images - WT

Click here to download high resolution image

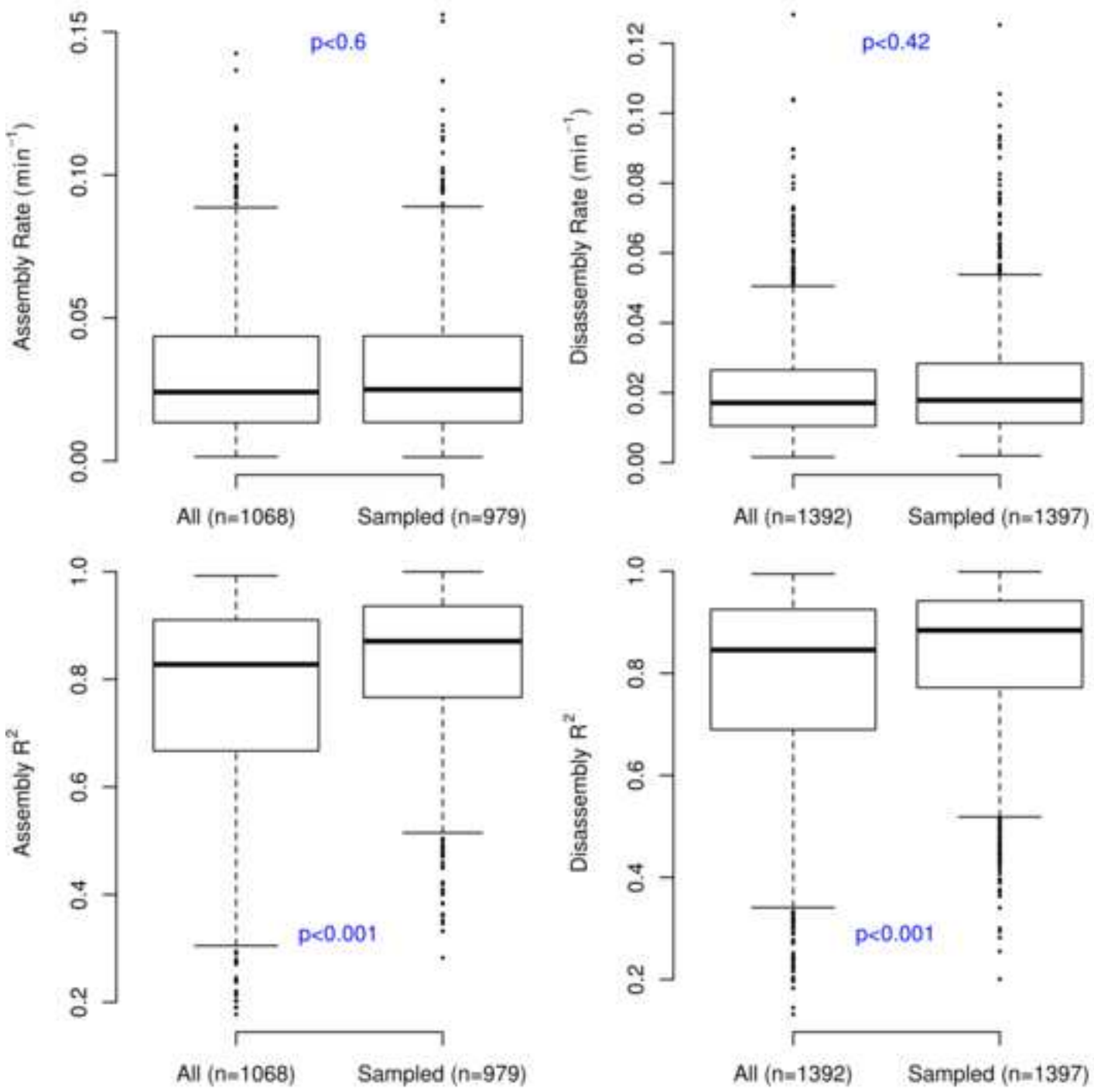

Figure S10. Sampled Images - S178A

Click here to download high resolution image

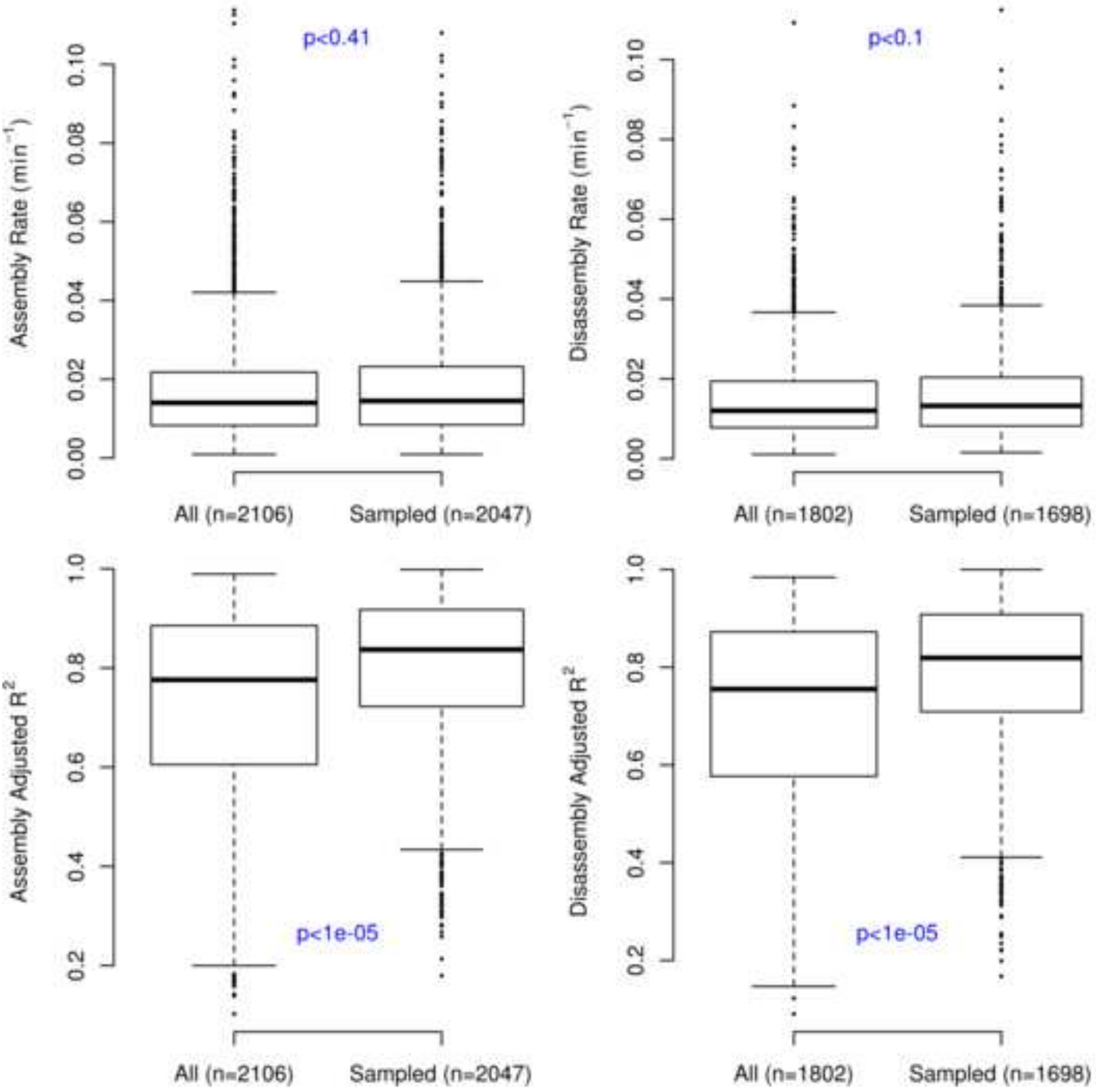

Figure S11. Simulation Stationary

Click here to download high resolution image

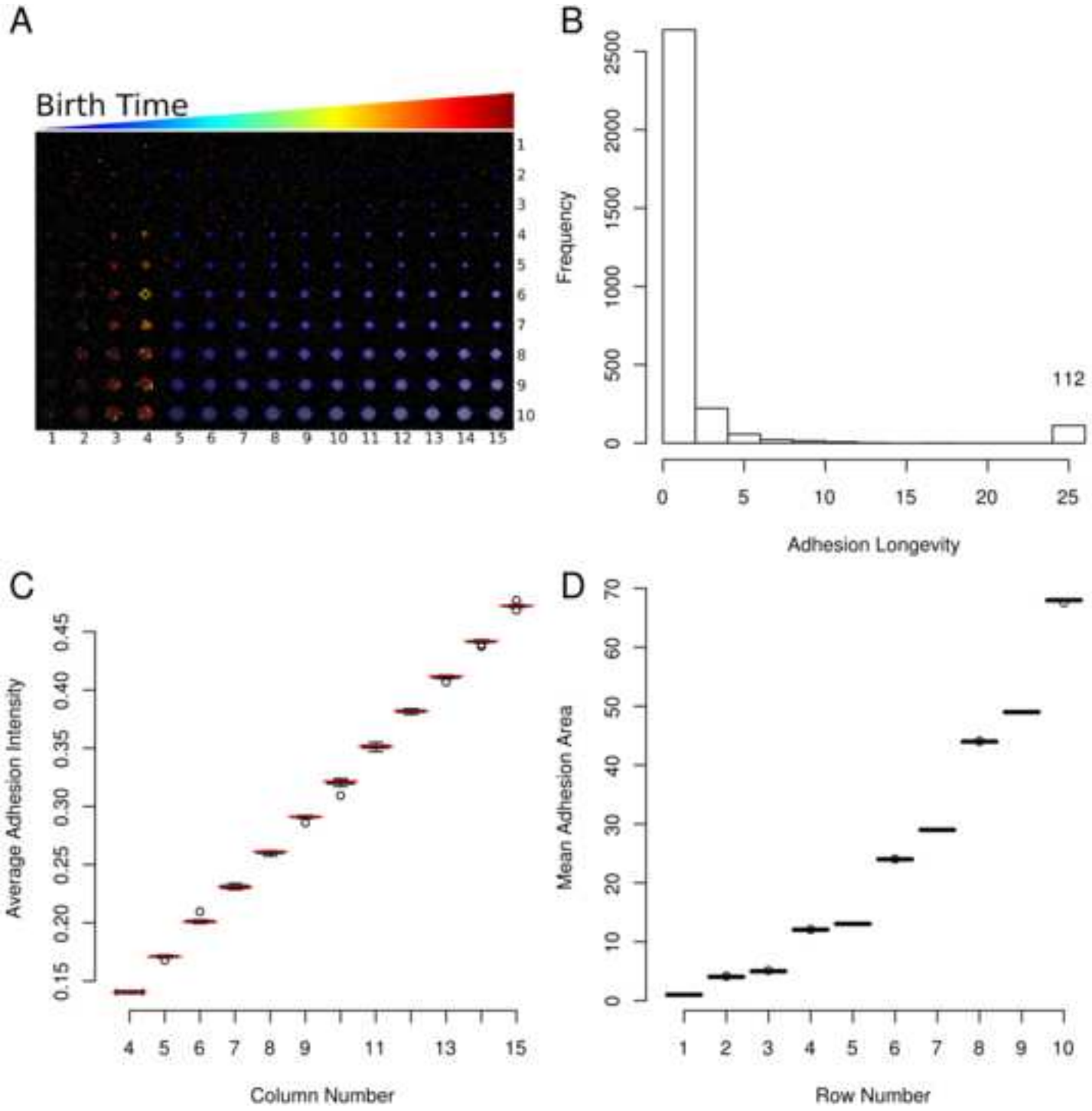

Figure S12. Simulation Moving
Click here to download high resolution image

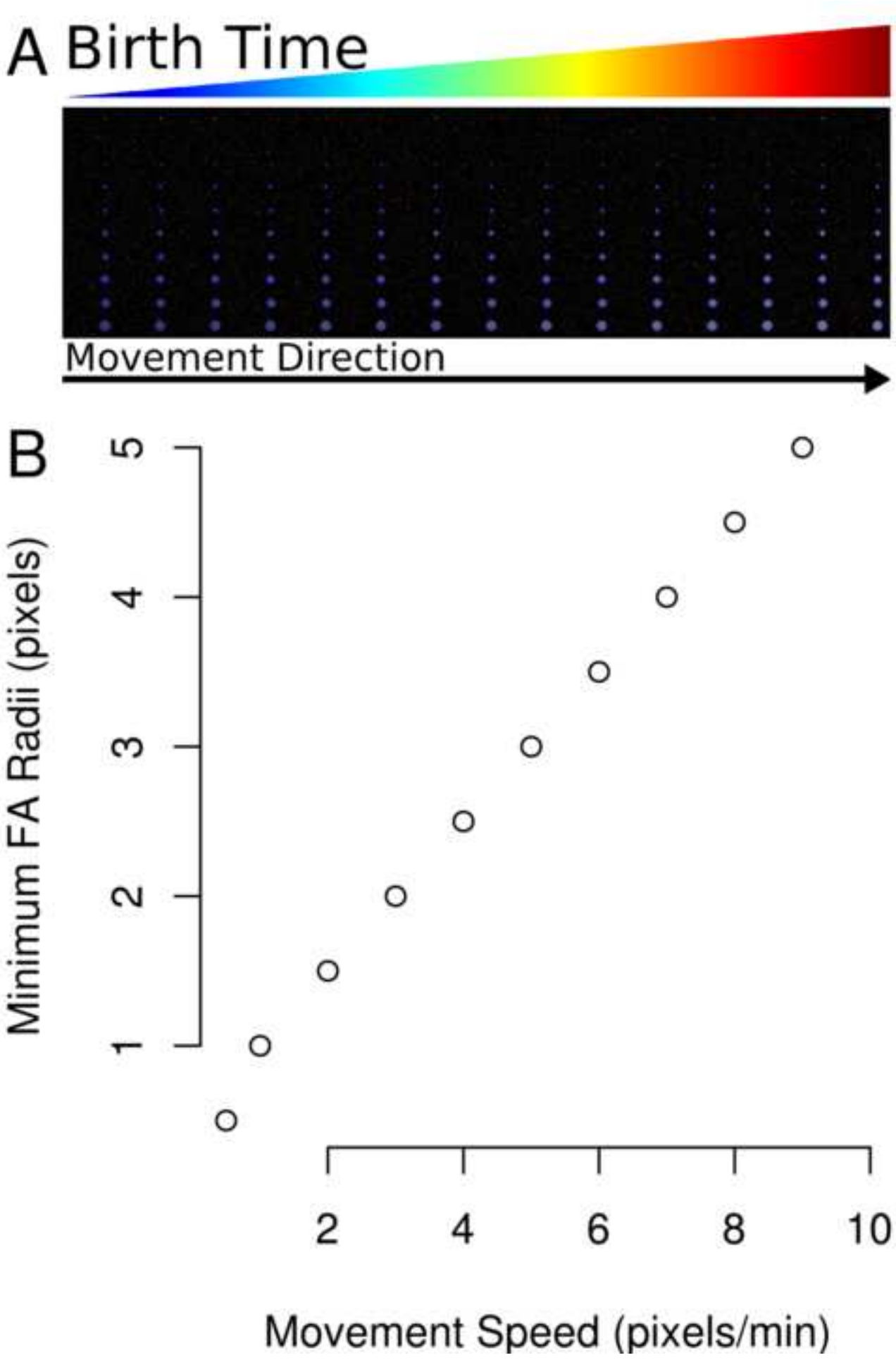

Figure S13. Simulation Kinetics

Click here to download high resolution image

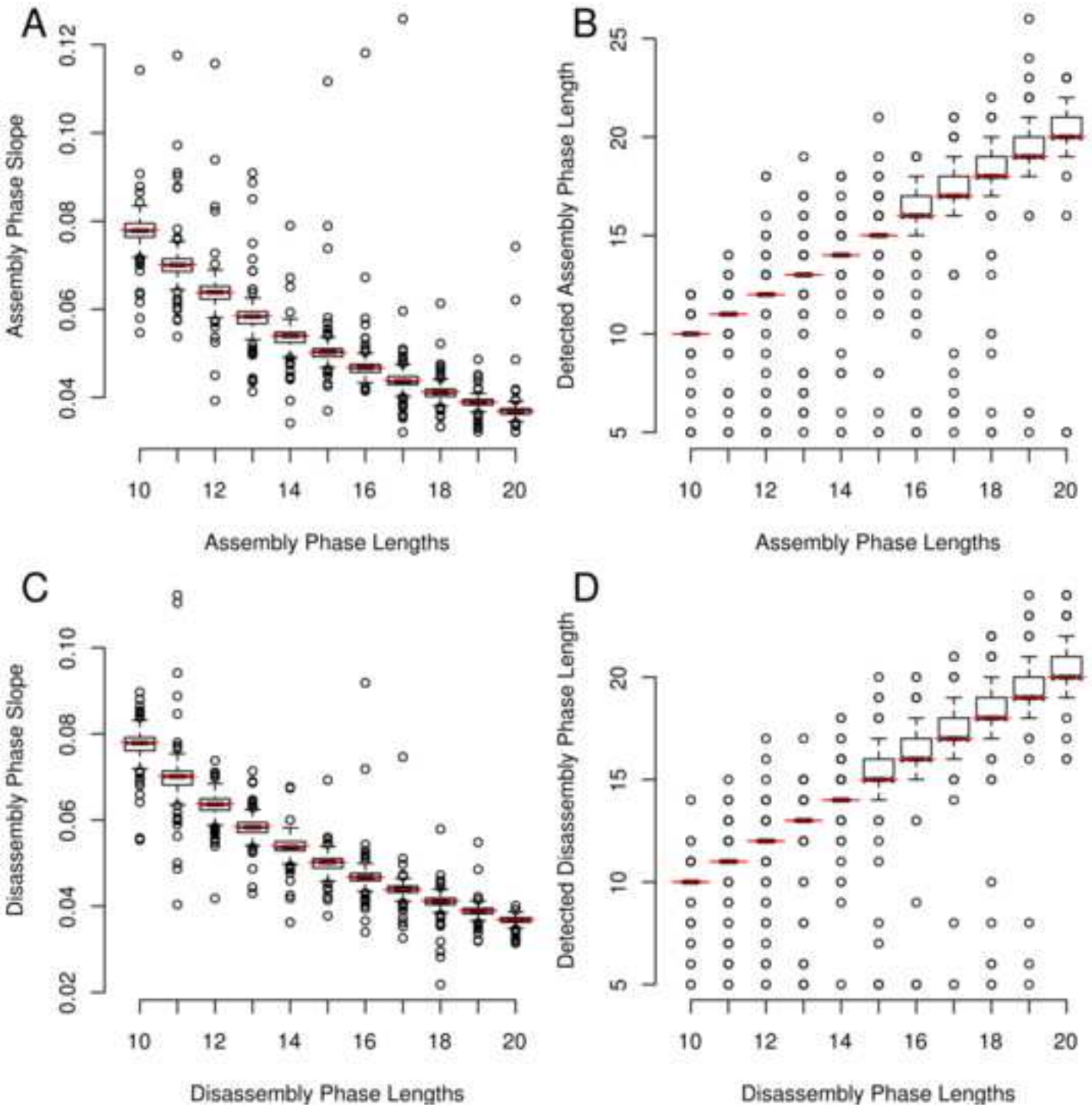

Movie S1. Sample Paxillin-EGFP Movie

Click here to download Supporting Information: Paxillin_sample.mov

Movie S2. Sample S178A-Paxillin-EGFP Movie

Click here to download Supporting Information: S178A_sample.mov

Movie S3. Sample FAK-EGFP Movie

Click here to download Supporting Information: FAK_sample.mov

Visualization of Full FA Time-lapse
Click here to download high resolution image

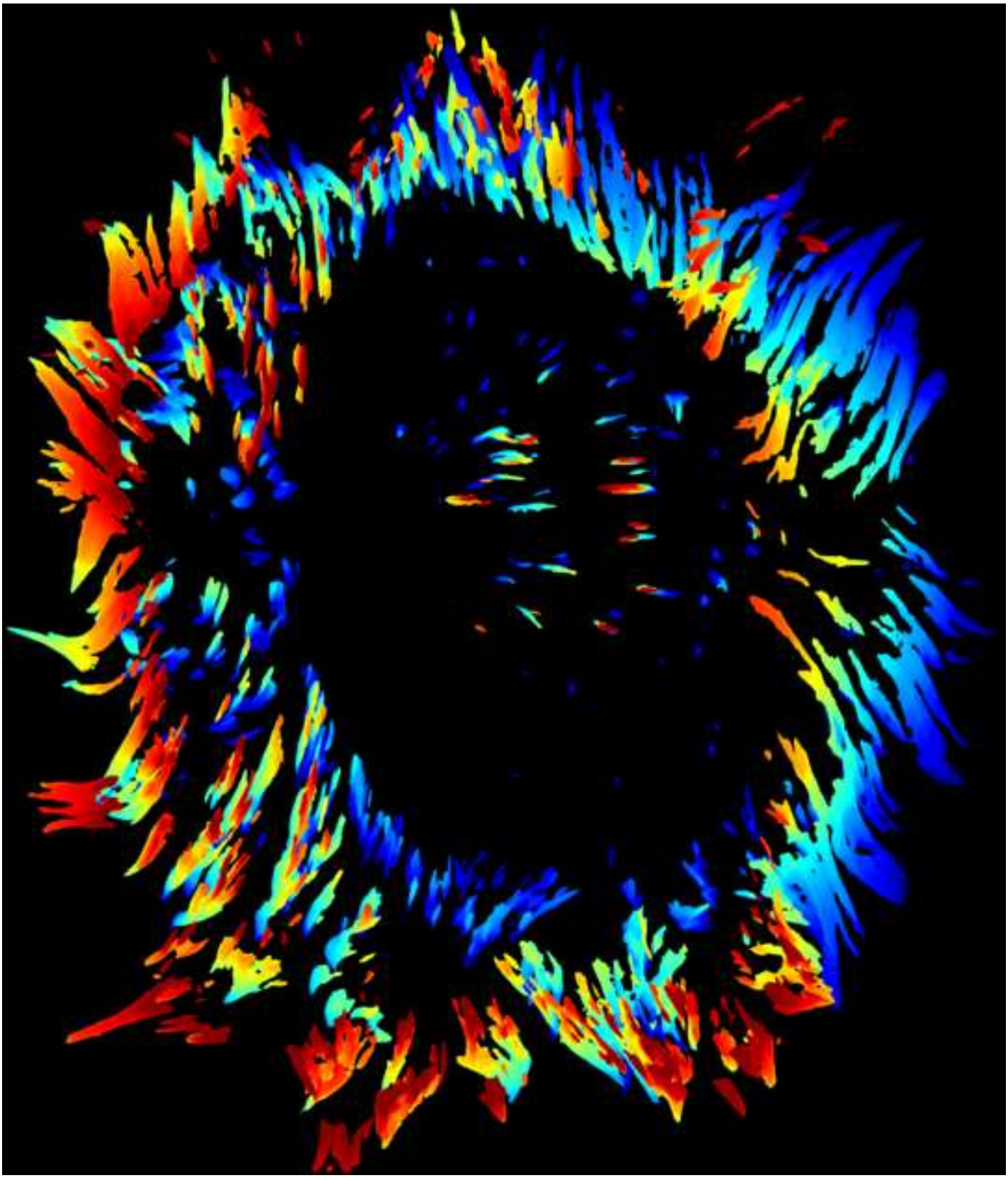

Detailed Response to Reviewer Comments for

"High-Resolution Quantification of Focal Adhesion Spatiotemporal Dynamics in Living Cells"
Matthew E. Berginski, Eric A. Vitriol, Klaus M. Hahn and Shawn M. Gomez

Reviewer #1:
Remarks for the Author:
In this paper, the authors present an elaborate study involving focal adhesion (FA) segmentation and quantification, as well as tracking of FA dynamics in live cells. They apply their analysis software for the characterization of the effects of mutating a major phosphorylation site in the FA protein paxillin on the structure, distribution and fate of the adhesion sites. The work presented here is, certainly, of high technical quality, and could potentially be useful for researchers working on FA dynamics. On the other hand - the novelty of this paper is rather limited, since FAs were segmented before, using a similar basic algorithms ("watershed-based"), and used for quantification of FA features in both fixed and live cells. The authors introduce a number of significant additions in the experimental design (e.g. use of TIRF illumination), as well as in the software, but whether these improvements are significant enough to justify a full publication - is questionable.

- We appreciate the positive comments, and do feel that there are multiple areas of novelty. From the computational standpoint, it is true that methods have been developed for identifying and quantifying FA features in cells. However, integration of identification, segmentation, tracking and analysis has not been done before for adhesions in live cells and this provides important new information and a new way to analyze adhesion function. Through this integration we have been able to quantify the dynamics of individual adhesions, as well as adhesion populations, on a scale that has not been previously attainable. Finally, we feel that this approach allows for the characterization of novel biology. For instance, in Figure 4 we are able to reveal relationships of assembly/disassembly in a spatial context, something that has not been demonstrated before. Similarly, demonstrating shifts in the position of an adhesion's place of birth due to a point mutation as well as other properties that we have quantified is inherently novel. Admittedly, further study is needed to provide a greater level of biological understanding. We hope that what we have shown some of this novelty as well as significant future potential.

The choice of paxillin mutation in S178 is a good one for demonstration of the power of the imaging the software - but the data shown here do not provide a meaningful contribution to the understanding of the role of this phosphorylation in regulating FA properties and dynamics, and merely serve as good demonstration of the quality of the software.

- We certainly agree that as a biological study, the work is by no means complete. However, we feel that our study does make a contribution to understanding the mechanism through which phosphorylation of Paxillin at Serine 178 affects adhesion behavior. One of the major goals of this work was to develop a system that could detect and quantify changes in adhesion properties that are difficult or impossible to do with current approaches. Properties having subtle changes, involving only specific

subpopulations, or changes in dynamics and/or spatial distributions often fall into this category. A primary goal with the Serine 178 mutation was to make a small perturbation to a single adhesion constituent to see how adhesion parameters were affected globally. A further rationale for this mutation choice is that this mutation was previously (and only qualitatively) described as having a strong effect on cell motility. To our knowledge, this is the first work that helps to explain why this change in motility may occur: through significant decreases in adhesion rates of assembly and disassembly. The finding of a spatial shift in adhesion birth position due to this mutation is also very intriguing, but awaits further specific investigation

Beyond these issues, the authors need to address a key problem associated with the segmentation of such structures as FAs - namely the basic definition of FAs. It is not clear what are the features on a paxillin-containing structure (intensity, size, shape) that qualifies it as a "focal complex" or "FA".

- The defining of what qualifies as a focal adhesion is a fundamentally tricky one as it is dependent on aspects such as the cell type, experimental setup as well as differences in definition between research groups. For instance, the Geiger group recently used a related imaging approach and siRNA screen to investigate FA properties within HeLa cells and defined an adhesion as “all distinct paxillin-containing structures larger than 0.25 sq microns (Winograd-Katz et al., 2009). In this manuscript, we avoid making the distinction between focal complexes and focal adhesions as the exact parameters that differentiate the two are based not only on size, but also on molecular composition. The Geiger group has even gone so far as to subcatagorize Focal Complexes into two groups (“Early” and “Late” Focal Complexes) based on their constituent components (reviewed in Zaidel-Bar et al. 2004). We simply state that we are able to examine the dynamic of adhesion complexes. These will of course be within a certain size range, determined by the limits of the microscopy technique used. Our goal in this study was to develop methods to obtain a completely unbiased survey of the adhesion profile of a migrating cell. We can identify any subpopulation of paxillin-containing structures based on size, shape, intensity, position in the cell, and dynamics (in any combination of the above variables), but in order to call these structures focal complexes, we would have to verify the presence (or absence) of certain adhesion components. This could be done with multi-color/ratio imaging and is a direction we plan on taking future research, but would be a study unto itself and outside the scope of this manuscript. We did perform an extensive sensitivity analysis and found that derived properties (e.g. the rates of assembly and disassembly) are not dependent on specific thresholds used to define and segment individual adhesions.

In conclusion - the technology looks good and potentially very useful for researchers (provided that the software is available for them), yet the novelty is limited. Taken together, I would recommend acceptance of the paper, under the condition that the software is made available to the scientific community (ideally - downloadable from the Journal's website).

- We realized that we had not made software availability explicitly clear in our earlier manuscript. The software is provided under an open source license and can be downloaded on our own website (http://gomezlab.bme.unc.edu/tools) where improved versions will also be provided. We would be happy to have it downloadable from the Journal's website as well.

Reviewer #2:

Remarks for the Author:

This manuscript describes a software application for the "unbiased" analysis of the position and dynamics of "all" the focal adhesions within cultured cells. This approach is reported to shorten data analysis times and avoid user-dependent selectivity issues. The focal adhesion protein paxillin and a previously described phospho-mutant were used in the analysis to provide proof of principle. Evidence is also presented that mutation of the S178 residue results in diminished focal adhesion turnover and position within the cell that could account for previously reported defects in cell migration. This is useful technology but there is little in the way of new mechanistic insight.

- The approach is as unbiased and comprehensive as we can readily imagine making it – labeled adhesions must have an intensity above a given level above background for them to be recognized, they are all tracked and their characteristics quantified in an equivalent manner.
- We feel that this method does far more than just shorten analysis times and avoid user-dependent selectivity issues. While in theory one could analyze the over 160,000 adhesion lineages measured across more than 5000 images, we feel that this not practically feasible. In addition, by comprehensively quantifying adhesions in live cells, we are able to establish adhesion properties that have not been defined previously, such as spatial position at birth and death. Furthermore, the ability to accurately measure large numbers of adhesions allows potentially subtle phenotypic changes to be analyzed in a statistically rigorous manner. The described approach should greatly enhance future focal adhesion studies.
- We do realize that there is much that needs to be done to use the new methodology to obtain mechanistic understanding of focal adhesion behavior and dynamics. We feel that the described approach provides a new tool that could aid many researchers in these efforts. This manuscript describes this tool (freely available), shows its performance on real data sets and its validation through simulated data sets, and provides an analysis of the S178A paxillin mutant showing the strong effects of this mutation on adhesion turnover with little change in other properties. It also indicates intriguing changes in adhesion dynamics (e.g. the shift in birth position due to the inability of JNK to phosphorylate S178) that warrant further studies. We plan to use this tool to understand underlying mechanisms in future experimental efforts.

Specific points

Cells expressing ectopic protein are used in this study, requiring multiple rounds of infection. Blots showing expression levels of WT and S178A as they relate to endogenous protein need to

be presented. Small changes in adhesions that re observed could be due to expression differences.

> We shared this concern as well – that the differences found between the Paxillin-EGFP and Paxillin$_{S178A}$ were potentially caused by a differential expression of the two fluorescently labeled adhesion components. To address this issue, we determined whole cell, cell background, and average adhesion fluorescence and determined all three parameters have no statistically detectable difference for cells expressing Paxillin-EGFP and Paxillin$_{S178A}$-EGFP. Thus, differences observed between the two cell lines are not due to differential expression. We have added Figure S3 to the publication showing these results.

Representative images of both sets of cells should be provided in order to valuate focal adhesion distribution. Movies used in the data acquisition should also be provided so we can evaluate the phenotype and dynamics of the cell over the extended time frame. How much photobleaching occurs during the course of a 4 hour TIRF movie? Is this correction incorporated into the intensity analysis?

- We have provided representative images as well as movies. The degree of photobleaching was assessed and was found to not be an issue. Regardless, correction for photobleaching is part of the standard image analysis process used in the manuscript.

It is hypothesized that the adhesions arise at the actin lammellipodia-lammella interface and that this position is changed by the S178A mutant. The authors are well qualified and equipped to test this with a fluorescently labeled actin probe and this should be done.

- The reviewer recommends conducting an experiment that would further support our observations concerning the underlying actin network changes around the shift from the birth to death adhesion regions. While we do feel this experiment would be highly interesting, the detailed study of the spatial distributions of adhesions under different conditions would require a separate dedicated study. We have tried to focus in this work solely on the characterization and quantification of adhesion dynamics. In future work, we plan to investigate the relationship between the spatial aspects of adhesion dynamics and key structures (e.g. at the lammellipodia-lamella interface) in normal adhesion behavior.

The mutant cells require 3 hrs to spread before imaging, but the WT cells are imaged after only 30 min. Are these really comparable? The WT cells are probably still spreading at this time. Thus any differences in distribution/turnover that are calculated may be more representative of the spreading status of the cell rather than the effect of the mutation. Cell populations should be spread for an extended period of time (overnight?) to reach equilibrium before they are imaged.

- We wanted to image the cells during migration, when adhesion turnover is highest. In our hands, these MEFs exhibit the best migratory phenotype 0.5-8hrs after being plated on fibronectin (right after spreading). It should be noted that while the S178A cells were given an extra 2.5 hrs to spread, the window in which they were imaged, 3-8hrs after plating, overlaps completely with the window in which WT cells were imaged (0.5-8hrs). Furthermore, in any given population of cells, there is a heterogeneous distribution of cells in different migratory states (spreading, migrating, quiescent, etc.). All cells were chosen for imaging based on their phenotype- a cell that had completed spreading and was now undergoing migration. Allowing the cells to sit overnight would result in cells with reduced migration, more quiescence, and less adhesion turnover.

I am not convinced that "all" adhesions are being imaged without user bias. Indeed, the authors clearly state they ignored short-lived adhesions-why? Are these not important to cell function? Also, what is the minimum size of adhesion can they detect/resolve with 2X2 binning? Furthermore, on P.18 it is reported that the user inserts a "specified length" in the calculation of assembly/disassembly.

- We filtered out short-lived adhesions only for the assembly and disassembly studies. The reason for this is that accurate quantification of assembly and disassembly requires that we see the process from beginning to end – from the birth of the adhesion all the way to it's death. Furthermore, to get accurate measures of assembly and disassembly, we need to have a sufficient number of measurements, both on the rise and fall of these curves, to make accurate fits to the data. As a result, we chose to require a minimum of 10 consecutive measurements of adhesion assembly, 10 consecutive measurements for disassembly and any number allowed in between. The "specified length" refers to this minimum of 10 observations in the assembly/disassembly phases. We also included a requirement to have observations of the adhesions' birth and death. Thus adhesions that could satisfy these criteria had to have a minimum lifetime of 20 minutes and short-lived adhesions were those that fell below this value. All other measures do not have this requirement and thus all adhesions are measured in these cases (given that they are of sufficient intensity relative to background to be detected and tracked). We do think that short-lived adhesions are important, but the accuracy of rate measurements requires us to place some conditions on the amount of data needed for fitting.
- The size of each pixel is 0.215 microns in length and since we report and track single pixel adhesions (after image filtering), the minimum size adhesion we can detect is 0.0462 square microns.

More mechanistic data is needed regarding how the S178A mutation affects adhesion dynamics. Otherwise these observations represent an incremental advance at best regarding our understanding of how phosphorylation of this residue affects paxillin function. The title of "key regulator" is overstated in the regard.

- We were not specifically clear enough on this point and our title was not correct in this regard. We have changed the title and demphasized the "key regulator" issue

mentioned. Our goal in this work was not to focus on this particular mutation or explain how phosphorylation of this residue affects paxillin function. Instead, we have focused on describing and validating a system for the analysis of focal adhesion spatiotemporal dynamics in living cells. As discussed in our response to Reveiwer 1, the use of the S178A mutation is a highly relevant system perturbation, with clear effects on global cell motility. We do realize that we have in no way explained all the mechanistic details of this mutation and its role in motility. We do, however, feel that it conclusively shows and quantifies previously undescribed effects of this mutation on adhesion dynamics. These results do help to explain previously described observations. Much work undoubtedly remains in describing the role of this phosphorylation site in adhesion dynamics as well as in other signaling events. We hope that this computational platform will help investigators studying this and related systems.

Detailed information regarding the statistical analysis is required. Some data sets seem to have extraordinary errors yet are show as being highly significant. For, example, in fig 5 mean area is less than 0.5 um but the errors are up to 14 in both the WT and S178A populations.

- We have added a "Statistical Tests" section within Methods and have clarified Figure 5, making it identical with all other box and whisker plots. For Figure 5, the top line of the box gives the 3rd quartile range and the whisker extends up to 1.5 times the interquartile range. Thus these are not really "error bars" but rather give a picture of the distribution of the data. An example of interpreting these would be that three quarters of the WT adhesions (panel A) have area less than 0.8 square microns (everything below the top line of the box). The bold central line gives the median value. Each of these bars is composed of over 300,000 data points and thus it is possible to detect subtle differences between distributions. We used a non-parametric Wilcoxon rank-sum test to assess the differences between distributions.

For this to be useful to the scientific community at large the authors need to provide more details regarding the software used and its availability.

- As discussed in response to Reviewer #1 above, we are making the complete software package available under an open-source license.

Reviewer #3:

Remarks for the Author:

This manuscript describes a new analysis system for the detection, tracking, and data extraction of adhesions in living cells. The analysis system is applied to quantifying the dynamics of the adhesion protein paxillin using total internal reflection fluorescence microscopy (TIR-FM). The authors analyze the size, shape, and intensity of paxillin- containing adhesions over time. They show that a paxillin mutant (S178A) affects the size, distribution, and rate of adhesion assembly.

This is a very nice study that develops a new method for quantifying the spatiotemporal dynamics of adhesions. The described method automates the collection and quantification of adhesion dynamics, making it feasible to analyze large numbers of adhesions, and should be of great interest and benefit to the research community.

- Again, we appreciate the positive comments and believe that this platform (freely downloadable and under an open-source license) will be of broad utility to the research community.

The data presented are convincing and show the feasibility and validity of the approach. However, the manuscript in its current form focuses more on technology development than on biological application. In addition, since on one adhesion protein (paxillin) was analyzed, their data indicates properties of paxillin assembly and disassembly, but cannot necessarily be extrapolated to adhesion assembly/disassembly in general. To address both of these concerns, the authors should analyze the spatial properties of the assembly and disassembly of another adhesion protein, such as vinculin. This analysis will strengthen this manuscript and allow the authors to provide a more general picture of the spatiotemporal dynamics of adhesions, which will increase the impact of this study.

Comments:

1. *In Figure 3A, is the scale bar 10 μm or 10 mm as indicated in the figure legend?*
    - It should be 10 microns – this has been corrected in the text.

2. An analysis similar to that done in Figure 4 should be performed with another adhesion protein, such as vinculin.

We have addressed the reviewer's concerns by adding Focal Adhesion Kinase (FAK), another key adhesion molecule, to our analysis. We did not have myr-RFP for our EGFP-FAK cells, which meant that edge detection had to be done through computational means. While we did do this, the results were noisier, so differences could not be confidently assessed for significance. In the end, we decided not to include the spatial comparison with FAK in this manuscript. Future work will address more fully the spatial dynamics of adhesions and adhesion components under different conditions/perturbations. Regardless, all other analyses could be performed and we found identical rates of assembly and disassembly for both Paxillin and FAK, and slight differences in their static properties (Figures in manuscript and supplemental materials). These results further support the methodologies and results found with the initial Paxillin-based experiments.